Hochschule
für Technik
Stuttgart

University of Applied Sciences

Master of Science Programme
Photogrammetry and Geoinformatics
Master Thesis
Winter Term 2021

Identification of alluvial gold mining in the Colombian Chocó region using radar satellite images

by

Leidy Johana Rico Trujillo

Supervisors: Prof. Dr Michael Hahn

Dr Thomas Esch

Identification of alluvial gold mining in the Colombian Chocó region using radar satellite images

by
Leidy Johana Rico Trujillo

A dissertation presented in partial fulfilment of the requirements for the degree of Master of Science in the Department of Geomatics, Computer Science and Mathematics, Stuttgart University of Applied Sciences

Declaration

The following Master thesis was prepared in my own words without any additional help. All used sources of literature are listed at the end of the thesis.

I hereby grant to Stuttgart University of Applied Sciences permission to reproduce and distribute publicly paper and electronic copies of this document in whole and in part.

Stuttgart, 28.02.2022

Leidy Johana Rico Trujillo

Approved by:

Prof. Dr. Michael Hahn

Acknowledgement

First, I want to thank life for challenging me to finish this new professional project. To my family in Colombia for their constant support and words of confidence, that reminds me that with willpower, anything is possible.

To my husband and his unconditional trust, this project would not have been possible without his support and inspiration.

I want to express special gratitude to Prof.Dr Michael Hahn and Dr Thomas Esch for agreeing to supervise my work and sharing their invaluable knowledge and experience on remote sensing and radar through their lectures.

Finally, my admiration to Prof. Dr Dietrich Schröder for allowing me to be part of the Master in Photogrammetry and Geoinformatics. To the Stuttgart University of Applied Sciences for providing the tools and equipment for the development of this work.

Master Course Photogrammetry and Geoinformatics

Identification of alluvial gold mining in the Colombian Chocó region using radar satellite images

Abstract

Alluvial gold mining is a growing activity in Colombia that severely impacts the loss of vegetation cover with high environmental value. The detection of this activity is essential to define strategies focused on reducing this impact. In previous studies that have used optical satellite imagery, continuous cloud cover, especially in tropical regions, has been a limiting factor that can be overcome thanks to the ability of radar sensors to capture information regardless of whether or illumination conditions.

In this project, time series analysis, textures metrics and supervised classification were implemented to identify areas affected by alluvial gold mining in the department of Choco. The approach involves two main steps: In the first, Sentinel-1 radar images with dual polarisation (HH and HV) and acquisition date between November 2020 and November 2021 were analysed, and in the second step, a TanDEM-X image with single polarisation (HH) was used. To evaluate the accuracy, classification results are compared with polygons identified in the region in 2021. The overall accuracy obtained was 97% with Sentinel-1 images and 98% with TanDEM-X. These results suggest that images used are suitable for identifying affected areas by alluvial gold mining. However, the discrimination of this affectation from the bare soil generated by other activities requires the inclusion of additional spatial criteria like the presence of previous affectation, beneficiation ponds and elevation data.

Keywords: SAR, Alluvial Gold Mining, Sentinel 1, TerraSAR-X, TanDEM-X, Time Series analysis

Table of content

List of Figures

List of Tables

Abbreviations

ACCA	Amazon Conservation
DLR	German Aerospace Centre
EC	European Commission
ESA	European Spatial Agency
GRD	Ground Range Detected
IDEAM	Hydrology, Meteorology and Environmental Studies of Colombia
NDI	Normalised Difference Index
SAR	Synthetic Aperture Radar
SIMCI	Sistema Integrado de Monitoreo de Cultivos Ilícitos
SLAR	Side-Looking Airborne Radar
UNODC	United Nations on Drugs and Crime

1 Introduction

Alluvial gold mining is a commercial activity that artisans have historically developed in Colombia. However, the increase in the price of gold in recent years has driven its transformation into a massive extraction practice using heavy machinery. These methods generate a high environmental impact associated with deforestation, removal of natural vegetation cover and mercury water contamination, among others (United Nations on Drugs and Crime. SIMCI 2021, p. 93).

The department of Choco, located in western Colombia, is one of the regions with the highest presence of this activity. The region has a unique ecosystem value, with comprehensive coverage of natural forests in which an intense rainfall regime predominates throughout the year (Arellano Peña, 2004, pp. 42-49).

The negative impact that this activity is causing on the environment has generated the need to develop methods for monitoring and characterising this phenomenon (United States Agency for International Development 2020, p. 1). In Colombia, the United Nations Office on Drugs and Crime (UNODC)-SIMCI Project undertook this challenge through alluvial gold evidence characterisation using optical satellite imagery since 2014.

In regions such as Chocó, the high cloud cover limits capturing information from optical systems during the whole year. It reduces the availability of information that can be incorporated into analyses.

In regions such as Chocó, the high cloud cover limits capturing information from optical systems during the whole year. It reduces the availability of information that can be incorporated into analyses.

Synthetic Aperture Radar (SAR) system is utilised to overcome the limitations of optical products in adverse weather conditions by providing cloud-free images. Several studies have investigated these images and have demonstrated their efficiency in land cover monitoring.

This thesis work aims to evaluate the radar satellite images to identify affected areas by alluvial gold mining in the department of Choco using intensity information of single and dual polarisation.

The proposed approach includes two main steps. In the first step, areas of land cover change were identified and extracted from the construction of a 1-year time series using Sentinel-1 imagery. The bare soil was identified within the change areas by applying a supervised classification with the Random Forest Classifier algorithm. Finally, areas affected by alluvial gold mining were determined based on an analysis of distances to previously affected areas and water bodies and the elevation ranges in which the phenomenon is usually located for this region.

In the second step, areas affected by alluvial gold mining were characterised by applying texture metrics and morphological filters to a TanDEM-X image with single polarisation (HH). After this process, a supervised classification was applied in which the elevation mask of the image was integrated for the identification of affected areas and water bodies associated with this activity. This process was completed using mainly the Sentinel Application Platform (SNAP) software produced by the European Space Agency (ESA).

The accuracy of the results obtained was evaluated using as reference information the polygons of affected areas by mining during the year 2021, provided by the UNODC - SIMCI Project in Colombia.

2 State of the art

This section shows the research work that has been conducted to investigate the application of satellite radar imagery in land cover monitoring and gold mining identification.

Although radar imagery has been on the market for several years, high acquisition costs and limited knowledge of processing techniques were for a long time a barrier to using these products in the development of environmental studies.

The release of Sentinel 1 images with free acquisition and the incorporation of processing algorithms in different software have increased the use of SAR products. However, their application to gold mining analysis has only recently begun to be explored.

Since 2014, the SIMCI Project has cooperated with the Colombian Ministry of Justice to establish a methodology for mapping, tracking and monitoring alluvial gold evidence on land and water using optical imagery and aerial overflights (United Nations on Drugs and Crime. SIMCI 2016). This work provided the baseline for the geo-referencing and characterisation of affected areas in the whole Colombian territory.

Since then, the project has published an annual report analysing the specific dynamics of the affectation and its influence on the change in vegetation cover. In addition, after 2018, it has incorporated evidence of alluvial gold in water detection by analysing spectral index to identify the presence of suspended sediments in water bodies (United Nations on Drugs and Crime. SIMCI 2019, p. 34)

In 2015 Saavedra S. initiated the development of a model that allows the detection of evidence gold mining using a machine learning algorithm with Landsat 8 satellite imagery. In 2019 this project was selected by Google as one of the 20 winners in the 'Artificial Intelligence for Social Good' competition (BBC News 2019). Saavedra is currently incorporating Sentinel 1 images to improve model prediction and is developing a web platform that will allow consultation of the information detected. According to Saavedra, "through this project, the model have been able to extract the patterns of open gold mines with 79% accuracy" (Ibid).

In 2016 the Institute of Hydrology, Meteorology and Environmental Studies of Colombia (IDEAM) started using Sentinel 1 image analysis to detect early deforestation alerts. This analysis has improved the tracking and monitoring of deforestation drivers in the Amazon Region. In this project, multi polarised images (VV and HH) have been integrated and analysed using principal components and synergies between Sentinel 1 and Sentinel 2 (IDEAM, 2016).

More recently, Ibrahima et al., 2020 implemented a Support Vector Machine (SVM) based on Sentinel 2 image classification with a Gaussian kernel to improve the identification of gold mining areas in the municipality of El Bagre (Antioquia, Colombia). This method achieved the sequential extraction of patterns that define the areas affected by gold mining and quantify the loss of vegetation caused between 2016 and 2019.

Barnabé et al., 2021 defined a workflow to identify and extract the potential direction of shadows at the sub-pixel level using Sentinel 2 imagery in areas with small-scale mining activities in Colombia. Using an approach based on the geometry and orientation of shadow projection on the ground, the authors automated cloud detection to improve the interpretation of areas with small-scale mining.

Regarding the use of the SAR system, Castro and Castillo, 2021, applied a time series and texture analysis to identify the footprint and machinery of excavation in gold mining areas in the municipality of Istmina (Chocó, Colombia). The research was done using SAR imagery from the commercial satellite Capella Space and ENVI SARscape® software. This study shows the usefulness of high-resolution radar data with improved radiometry and low speckle levels for monitoring and alert generation in areas with high cloud cover in the Colombian Pacific Region.

(Conservacion Amazónica-ACCA), in 2021, developed a web service for monitoring and detecting early warnings of deforestation due to gold mining in Peru. By applying a change detection algorithm on Sentinel 1 radar images, affected areas were detected. In addition, it published a geographic web visor through which it is possible to consult spatial information and perform spatial operations at different scales. This platform provides information on the progress of gold mining in the Peruvian Amazon, which can improve the planning for the control of illegal mining and forest damage.

Adamek et al., 2021, applied vegetation and geological indexes on Sentinel 2 and Landsat 8 imagery to identify and quantify areas degraded by gold mining in the Madre de Dios region of Peru. The process was performed using a semi-automatic classification plugin of QGIS, and the main result was the spatial distribution of minerals and sulphates exposed in gold mining areas.

Other studies have implemented the use of radar focused on quantifying forest loss rather than characterising gold mining areas. Among these are Almeida-Filho and Shimabukuro Y., 2010. They evaluated the usefulness of JERS-1 radar imagery in conjunction with applying the Normalised Difference Index (NDI) to identify and quantify disturbed areas by gold mining extraction in the Serra Tepequem region, Roraima (Brazil).

Joshi et al., 2015 demonstrated the usefulness of ALOS PALSAR (L-band) radar imagery for detecting deforestation and tropical forest degradation. This work characterised forest disturbance by identifying the backscatter values of different deforestation events between 2017 and 2018 in Tahuamanu and Tambopata (Madre de Dios, Peru).

Isidro et al., 2017 identified the footprint of small-scale mining in the Cagayan region of northeastern Philippines. In this work, a workflow for the segmentation of Landsat 8, SPOT 6 and Pleiades-1A optical images were created using the OB-SVM algorithm of the ENVI software, which provides a knowledge base of these areas in tropical rainforest ecosystems.

Jaelani et al., 2018 used classification methods with Sentinel 1A imagery to determine the change in vegetation cover generated by gold mining between 2015 and 2017 in the Bombana region, located in Southeast Indonesia.

3 Theoretical Background

The current work is based on the concepts of geometry and characteristics of SAR systems and the techniques applied for distortion correction and image processing. This section includes a description of the geometrical and radiometric properties of radar images and classification methods implemented.

3.1 Synthetic Aperture Radar

Radar systems have been developed rapidly since World War II and were initially used for military and navigational purposes. The echo of the signal emitted by the sensor allowed the identification of moving objects (Curlander and Mcdonough, 1991, pp. 26-28).

After the War, its applications focused on traffic control (maritime and air) and the monitoring of meteorological phenomena. In the 1950s, with the appearance of Side-Looking Airborne Radar (SLAR) systems, the development of SAR began. With them, images capture is useful for monitoring and observing the Earth's surface (Ibid. pp. 31–38).

Since then, different international agencies and entities have focused on the study and development of new radar systems that facilitate the capture of images for the monitoring and analysis of environmental phenomena (fires, deforestation, floods, among others) and the administration of natural resources in different areas of the world.

SAR systems are active sensors that emit a pulse of energy and measure the backscatter generated when the electromagnetic wave strikes objects on the Earth's surface. This scattering depends on the amplitude, phase and polarisation of the wave (Ibid. p. 45).

Wave scattering provides information about the surface characteristics as a function of three parameters: "the roughness (how much of the scattered radar energy is directed back to the sensor), the dielectric constant (how deep signals

may penetrate the scattering surface) and the local slope" (Flores et al., 2019, p. 25).

The images captured by the system store information with different wavelengths called bands. These wavelengths affect the penetration capacity of the signal in the surface so that "longer wavelengths (P and L bands) penetrate deeper into vegetation canopies and soil" (Ibid et al. p. 29). The application and use of each band are defined according to the frequency and wavelength that characterises them (Table 1).

Band	Frequency (GHz)	Wavelength (cm)	Applications
X	8 -12	3.8-2.4	High-resolution (urban monitoring; ice and snow, little penetration into vegetation cover)
C	4 – 8	7.5-3.8	Global mapping, change detection, monitoring of areas with low to moderate vegetation Improved penetration, higher coherence, ice, ocean
S	2 – 4	15-7.5	Little but increasing use for SAR-based Earth observation, agriculture monitoring (NISAR will carry an S-band channel. Expands C-band applications to higher vegetation density)
L	1 – 2	30-15	Medium resolution SAR (Geophysical monitoring, biomass and vegetation mapping, high penetration, InSAR)
P	0.3 - 1	100-30	Biomass. The first P-band spaceborne SAR launched in 2020. Vegetation mapping and assessment. Experimental SAR.

Table 1. Microwave bands for SAR System.
Taken from: (Flores et al. 2019, p. 29)

The frequency range in which the SAR system operates has 100% transmission through the oxygen and water vapour molecules present in the atmosphere (Figure

1). Together with the "geometric resolution independent of sensor altitude or wavelength imaging" (Curlander and Mcdonough, 1991, p. 4), these characteristics guarantee the continuous capture of images with high resolution and constitute the main advantages of using this system over optical sensors.

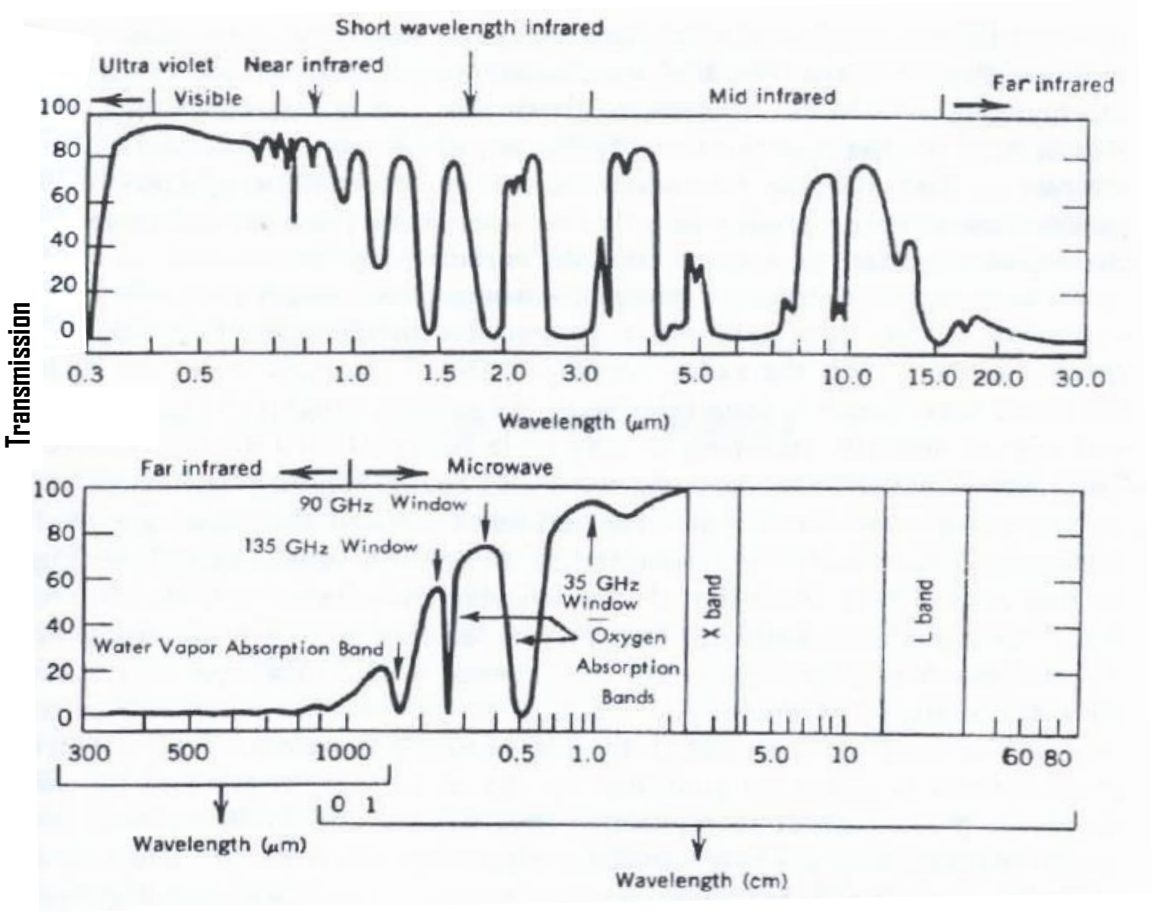

Figure 1. Percentage of transmission through the atmosphere.

For the range between 3-30 cm length (X to L bands), the transmissivity is close to 100%. Taken from: (Curlander and Mcdonough 1991, p. 5)

3.2 Geometric properties of SAR images

Radar data are affected by geometric distortions produced due to the inherent side-looking nature of radar, the slope and other characteristics of the terrain illuminated by the sensor. The central distortions presented by radar images are:

a. Foreshortening: this distortion occurs when the radar beam hits a slope oriented towards the sensor. As radar measures distance in slant range, the slope is compressed, and the length of the slope is incorrectly represented in the image.

   The intensity of this effect depends on the angle of the mountain slope and its relationship to the incidence angle of the radar beam to reach its maximum when the two angles are equal.

   The foreshortened slopes on the image appear as bright features and slope towards the radar. This distortion can be reduced by using images with large angles of incidence (close to 45°), and the effect on the images can be corrected by the geocoding process, using a DEM (Flores et al., 2019, pp. 23-24).

b. Layover occurs when the return signal from the upper part of the relief is received before the signal from the lower part. As a result, the mountain top is displaced towards the radar and located above the feature base (terrain inversion). As with foreshortening, this effect generates bright tones in the image, and the intensity of the effect is higher for small angles of incidence and in mountainous terrain.

c. Shadow is produced when the relief slopes are hidden from view, generating no return echo. In this effect, the angle of observation is greater than the inclination angle. This effect is represented as dark areas where the image receives no information (Ibid et al. pp. 23-24).

Although image distortions associated with topography cannot be eliminated entirely, it is possible to apply some correction techniques to minimise the effect of these on images. The geometric distortions are shown in Figure 2.

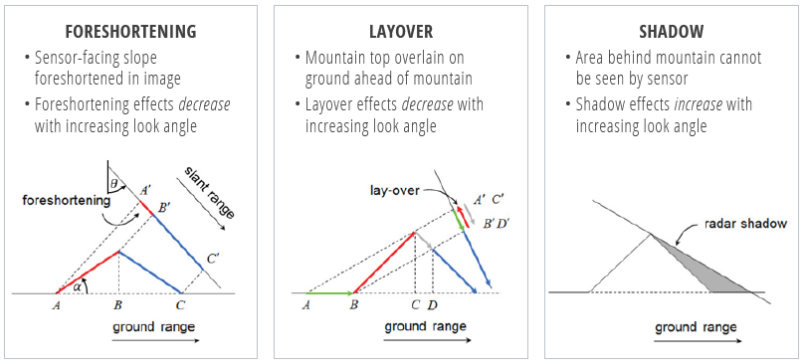

Figure 2. Main geometric distortions that affect radar data

Taken from: (Flores et al., 2019, p. 24)

3.3 Radiometric properties of SAR images

SAR images are monochromatic, and the brightness of the pixel is directly related to the reflectivity of the terrain illuminated by the radar. Radiometric values range from entirely dark to completely bright. In this sense, if an object or surface reflects a large part of the incident radar energy towards the sensor, this pixel will have a high digital value and be represented with a white tone. If an object does not reflect much energy, it will have a low digital value and be represented as black.

The radar signal is emitted in-phase coherently without interference when this signal interacts with the illuminated object, it is no longer in-phase, and the waves produce interference (constructive and destructive) that generates light and dark pixels called speckle, which is represented in the images as a grainy or 'salt and pepper' effect (Flores et al., 2019, pp. 24-25).

The speckle can be treated mathematically as a random noise factor overlapping the radar signal. This noise does not significantly alter the average signal strength in homogeneous areas. This feature can be used for speckle reduction by calculating the average values of neighbouring cells; this process impacts the reduction of the spatial resolution of the image.

There are different methods of speckle reduction, the main ones are described below, and the application of one or more of these depends on the objectives of the analysis done with the radar images:

1. Multi-look processing: in a SAR image, each transmitted pulse is represented as a line of cells in the range direction; these lines are known as 'looks'. The dimensions of a look are not the same in the azimuth and range direction because different SAR characteristics control the resolution in each direction. A single look image cell is often longer in the range direction than the azimuth direction.

   This method merges small groups of adjacent range lines to produce a new square-shaped line with values recalculated by averaging the azimuth direction. The resulting image has reduced speckle and better geometric characteristics.

2. Speckle filters: In this method, a measure for the noise range (standard deviation) is estimated from the actual brightness variations of the image by using the local pixels within a filter window defined according to the analysis objectives. This process aims to reduce speckle noise in uniform regions by averaging the values while preserving the brightness variations at the boundaries of areas with different overall brightness.

These filters result in blurred or loss of spatial detail in the image. The size of the filter kernel should be determined as a function of the trade-off between noise reduction and appropriate loss of spatial resolution (Microimages, 2012, pp 14-16). Figure 3 shows a scheme of speckle formation from the constructive and destructive waves.

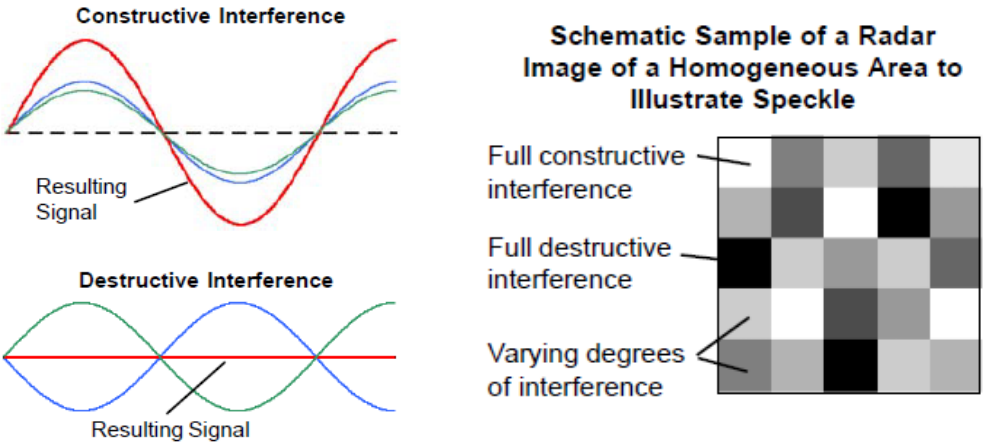

Figure 3. Constructive and destructive interference in speckle formation
Taken from: (Microimages, 2012, p.14)

3.4 SAR scene parameters

Radar intensity depends on several factors such as surface orientation, surface roughness, dielectric properties, and the radar wave's polarisation direction.

Surface roughness is the main characteristic that determines the radar response in flat areas; a smooth horizontal surface, such as a calm body of water, acts as a mirror, producing a specular reflection. In these cases, the energy returning to the radar is low, and therefore the smooth areas appear in dark tones such as rivers and other bodies of water.

When the signal hits an irregular surface, it scatters the energy in different directions. Some of the scattered energy returns to the radar, where its detection produces a bright response in the image. Hence, the brightness increases with the degree of roughness of the illuminated surface.

Roughness refers to the degree of irregularity and vertical relief of surfaces. If a surface appears rough in a radar image, this depends mainly on the radar's wavelength. "According to the Fraunhofer criterion, a surface is defined as rough if the height deviations exceed the value h rough, which is determined by the equation: through > λ / ((32 - cosθi))." (Flores et al., 2019, p.26).

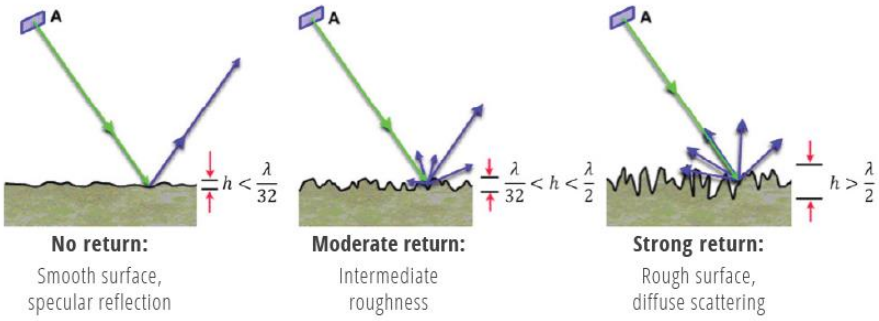

Figure 4. Relationship between surface roughness and radar wavelength

Taken from: (Flores et al., 2019, p. 27)

On the other hand, the dielectric properties of a medium define how the signal interacts with a scattering surface. These properties determine the amount of incoming scattered radiation, the quantity of energy that penetrates the medium and the final energy absorbed.

The signal penetration depends on the wavelength; according to this, radar penetration is more profound as the wavelength increases. The L-band has a longer wavelength and, therefore, greater penetration than the C- or X-bands. This dynamic means that X-band sensors in vegetation areas are mainly scattered in the treetops, whereas C- and L-bands can penetrate down to the ground level (Flores et al., 2019, pp. 26-30). For example, the X-band signals are scattered close to the surface on bare surfaces, such as alluvial soils or glacier ice. At the same time, the C- and L-bands penetrate progressively into this environment.

The sensor frequency is proportional to the wavelength; in this sense, when the frequency increases, wavelength decreases and therefore, the penetration depth into the medium drops.

Since the SAR is an active system (with its light source), it is possible to completely control the signal's polarisation, which defines the orientation of the plane in which the signal propagates. SAR sensors include single-polarized sensors that work with a linear polarisation HH (transmits and receives horizontally) or VV (transmits and receives vertically). Additionally, cross-polarized sensors transmit the signal in one plane and receive it in another, HV (transmits horizontally and receives vertically) or VH (transmits vertically and receives horizontally).

The backscattering mechanism can be of three types depending on the illuminated surface: 1. Rough surface scattering, in which most of the scattered energy returning to the antenna has the same polarisation as the transmitted signal. This characteristic is common in areas with little vegetation and bare ground, roads and asphalt surfaces. 2. double-bounce scattering, which occurs for buildings, tree trunks and other vertical structures that deflect a first reflection forward of the sensor; and 3. volume scatterers whereby the signal is partially depolarised so that some of the scattered waves oscillate in several directions (Ibid et al., 2019, pp. 26 -30).

This behaviour occurs, for example, with tree canopies as the signal bounces multiple times on its propagation path through the vegetation structure.

3.5 Radar polarisation and scattering

SAR systems transmit a polarisation pulse that usually oscillates in a plane perpendicular to the direction in which the wave is transmitted. The most common polarisation mode transmits and receives the signal on the horizontal plane.

However, when the radar pulse hits the vegetation, there is decomposition in the signal resulting from the interaction with the different structures such as leaves, twigs and branches; this decomposition causes the radar signal to pulse in different directions and produces a volume scattering that can provide information about the structures on the illuminated surface.

Some radar systems, such as Sentinel 1, transmit and receive vertical and horizontal polarisation (dual polarisation). From this information, cross-polarised images are generated, for these, the signal has been sent in one direction, and the reception and recording of the returned pulse have been done in the perpendicular direction.

The main scattering mechanisms are surface, volume and double-bounce scattering. Surface scattering occurs mainly when there is exposed soil or no vegetation. The low level of energy received by the antenna in these cases causes these areas to have dark tones in the radar images.

Volume scattering commonly occurs when there is vegetation, and double bounce scattering occurs when there are two perpendicular surfaces, such as in urban areas where there are streets and buildings on either side.

The decomposition of these polarimetries helps obtain information about the structures of the analysed surface and providing criteria for differentiation between these surfaces.

3.6 Supervised classification methods.

Different classification methods have been explored and evaluated to identify coverages from SAR images. The quality of the classification results depends on the robustness of the classifier, the quality of the input features and the sufficiency of the training samples.

One of the most widely used and studied methods in the last decades is the Random Forest classifier; this method has fast execution and consists of a collection of decision trees generated with the samples and subsets of training data.

The output class is defined according to the decisions made in order of importance for each pixel. This generates a ramification of decisions since to make a final decision, each tree has a vote.

This method introduces randomness into the model for tree growth, which implies that instead of looking for the most important feature in splitting a node, it chooses the best feature from among a random subset of characteristics (Ho, pp. 1-3).

One of the advantages of the random forest is that it can be used for regression and classification tasks. The random decision tree is composed of three elements: decision nodes, leaf nodes and a root node. The algorithm divides a training dataset into branches, which in turn are subdivided into further branches until a leaf node is reached, which can no longer be divided (Breiman, 2001, pp. 11-16).

The final class is selected based on the most common decision made by all random decision trees. Figure 5 shows the three types of nodes used by the random forest classifier:

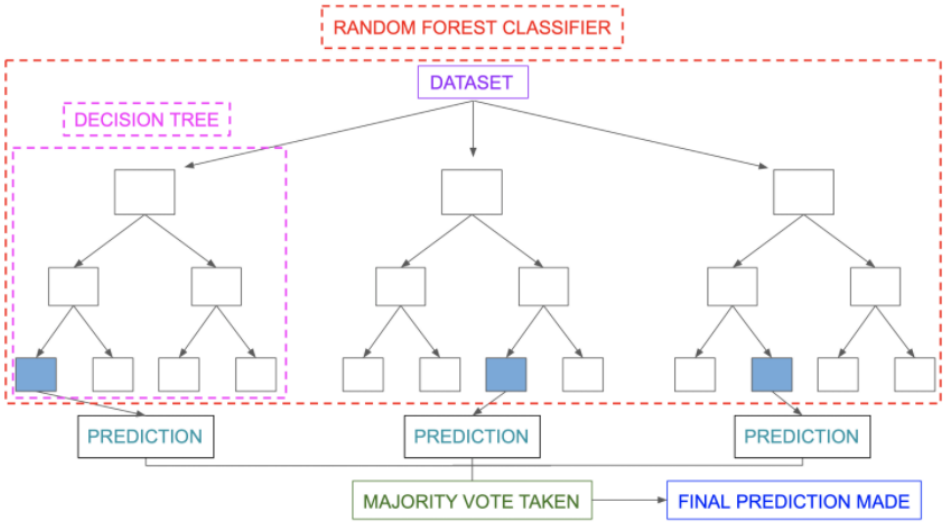

Figure 5. Random forest classifier decision scheme
Taken from: https://www.section.io/engineering-education/introduction-to-random-forest-in-machine-learning/

3.7 Texture analysis

Texture usually refers to the spatial variation of the tones or brightness of the pixels in an image. Different types of textures can be extracted and analysed to enhance and identify the spatial patterns of an element in SAR images.

Haralick describes the use of 14 texture types and how they contain essential information about the structure of surfaces and their relationship to the surrounding environment. Texture and tone are always present in the image so that when a portion of the image has slight variations in tone, the dominant property is tone. However, when the variation in grey tones is significant, the dominant property in that area will be texture (Haralick et al. 1973, pp. 610-612).

Texture analysis is often used to improve the classification of coverages in radar images; however the optimal texture type depends on the kind of coverage analysed. Most studies suggest that the best results are obtained by calculating Grey Level Co-occurrence Matrix (GLCM) texture measures that consider the relationship between two pixels called the reference and the neighbour pixel (Hall-Beyer 2005, pp. 2-12).

The texture measures are divided into three groups:

1. Contrast group: in this group are defined contrast and homogeneity for which if the weights decrease over the diagonal, the calculated texture will be significant for windows with little contrast. Another measure is Dissimilarity, for which the weights increase linearly.

2. Related to orderliness: in this category are grouped measures in which the weight is based on how many times a given pair occurs in such a way that "weight that *in*creases with commonness will yield a texture measure that *in*creases with orderliness. A weight that *de*creases with commonness yields a texture measure that increases with *dis*order" (Hall-Beyer 2005, p. 36). This group contains the angular second moment (ASM), energy, MAX and entropy.

3. Descriptive Statistics of GLCM: This group uses equations similar to basic descriptive statistics such as mean or standard deviation calculated from the GLCM values and not from the original pixel values. Within this group are Mean, calculated as the weighting of the pixel by its frequency of occurrence combined with a given neighbouring pixel value.

   Variance is based on the mean and dispersion using the combinations of reference pixels and their neighbours. And finally, the correlation, which measures the linear dependency of the grey levels on those of the neighbouring pixels. (Hall-Beyer 2005, pp. 36-43).

3.8 Accuracy evaluation

Accuracy assessment quantifies the correctness of the classification result data set that is useful for evaluating the classification approach used and determining the error that may be involved in this process.

The evaluation is done by statistically comparing the reference data representing the ground truth with the respective class obtained as a result. One of the most commonly used methods is the confusion matrix, which can be applied to binary classifications and multiple classification problems.

Through this matrix, different metrics are calculated (L3 Harris TM. Geospatial):

- Overall accuracy, which represents the proportion of correctly classified samples and is calculated using the expression:

$$OA = \frac{\text{Number of correctly classified samples}}{\text{Number of samples}}$$

- The accuracy of the user representing the accuracies for each class from the map user's point of view.

$$UA\ class1 = \frac{\text{Number of correctly classified samples of class 1}}{\text{Sum of samples classified as class1}}$$

- The accuracy of productor, which provides the accuracy per class from the map maker point of view.

$$PA\ class1 = \frac{\text{Number of correctly classified samples of class 1}}{\text{Sum of samples with true label of class1}}$$

4 Objectives

The primary goal of this work is to define a methodology to detect and quantify areas affected by alluvial gold mining along rivers and streams in the department of Choco, Colombia, using radar remote sensing.

The study aims to implement a two-stage analysis workflow to achieve this goal. In a first step, radar images from the 10 m Sentinel 1 sensor will be used for a large-area scanning and monitoring of the Choco department. This procedure shall provide a map of hotspots and areas with a high concentration of alluvial gold mining activities.

In the second analytics step, high-resolution TerraSAR-X radar images (1-3 m) will then be employed to identify and characterise the spatial patterns of the mining footprint within the candidate areas identified in the initial step.

Finally, the outcomes will be validated based on a vector layer with the alluvial gold mining evidence in 2021, generated by United Nations (SIMCI Project) in Colombia which will serve as a reference or ground truth layer.

5 Methodology

This section describes in detail the study area, the data used for the analysis and the objectives defined for the development of this work.

In addition, the methodology used is described, which was applied following three main stages: 1. Image pre-processing, by which images for the study area were downloaded, and the necessary operations were applied to reduce the noise and distortions of the original images. 2. The processing, through which the time series analysis, texture extraction and thematic classification of the images were performed. And 3. Post-processing, in which was performed the classification

edition, construction of final land cover mosaic, the evaluation of the accuracy and the analysis of the results. The overall workflow is shown in Figure 6.

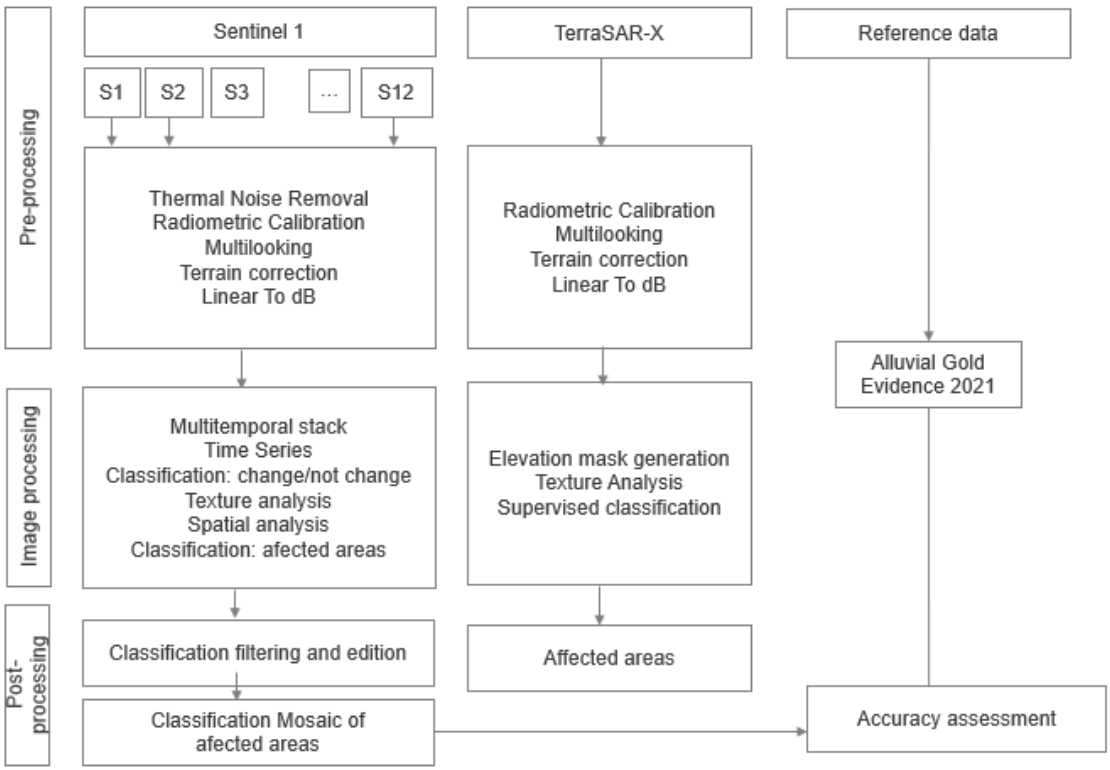

Figure 6. General workflow to identify affected areas by alluvial gold mining

5.1 Study Area

The study area is located in the department of Choco, over the Pacific Colombian region, Figure 7. This department has a total area of 46,530 Km^2. 7% of this area (3,250 km^2) corresponds to tropical forest cover, and 30% is considered a protected area due to its high ecosystem and environmental value(IDEAM. Subdireccion de Ecosistemas e Información Ambiental 2015).

Due to its location, Choco has an intense rainfall regime that varies between 5,000 mm and 9,000 mm and approximately 200 rainy days per year. This rainfall regime, combined with a warm humid climate with temperatures between 26 and 28

degrees Celsius, generates extensive cloud cover throughout the year in the department (Guzmán D. et al. 2014, p. 31).

According to UNODC, in 2020, Chocó was the second most affected department in Colombia by alluvial gold mining. During that year, the department concentrated 36% of the national affected area, which generates a loss of approximately 16 Km^2 of forest per year (United Nations on Drugs and Crime. SIMCI 2021, p. 94).

For the analysis developed in this work, an area of 11.160 Km^2 was selected where, according to UNODC-SIMCI Project reports, the highest concentration of alluvial gold affectation is located. In Figure 7, the area of interest is shown in green.

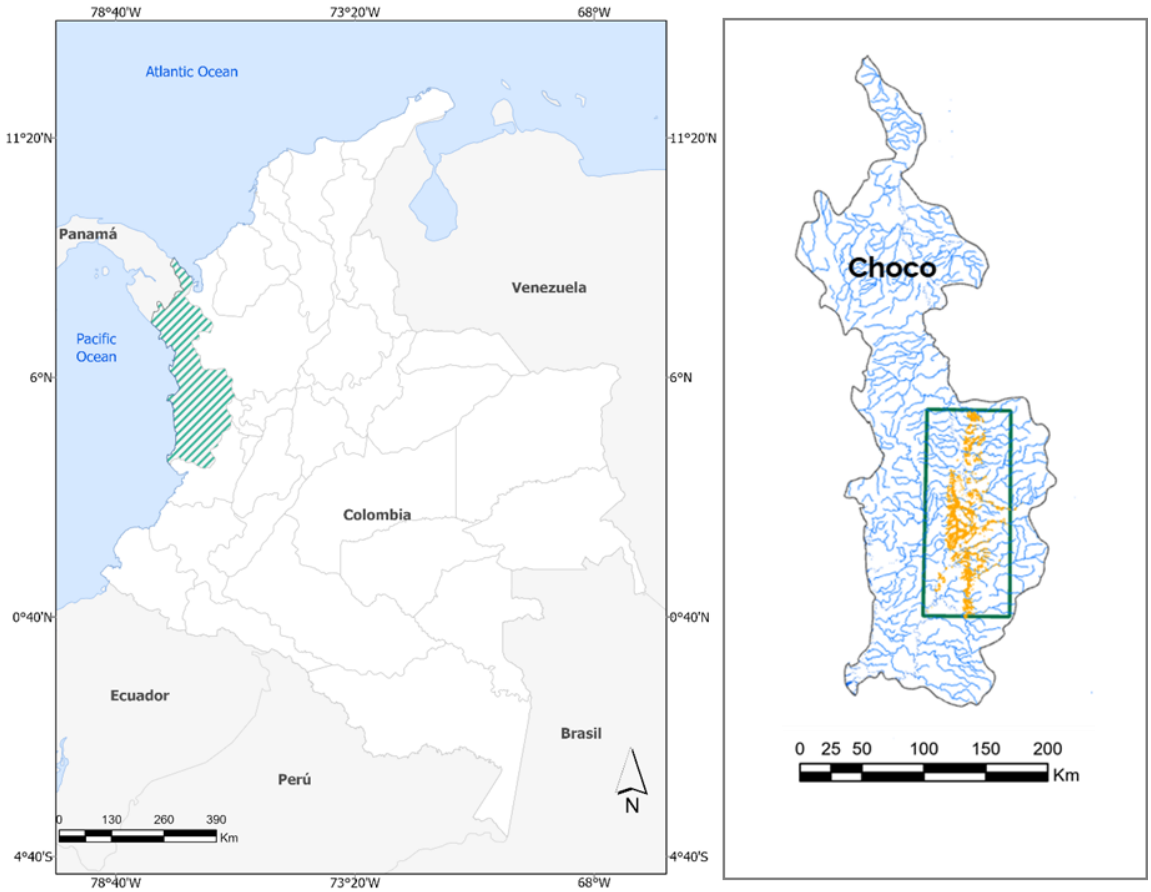

Figure 7. Choco department location

5.2 Data and software

The three types of data and software used in this work are described as follows

5.2.1 Sentinel 1

The Sentinel 1 mission was an initiative between the Copernicus project of the European Commission (EC) and the ESA that aims to provide continuous data for analysis and monitoring of the land and ocean.

The mission is composed of two satellites (Sentinel 1A and Sentinel 1B) that share the same orbit and guarantees a revising time of 6 days for the entire surface of the Earth. "These satellites work with SAR technology and capture information using C-band that supports dual polarisation operation (HH + HV, VV + VH), which is useful for land cover classification and monitoring" (The European Space Agency 2021, pp. 6–9).

The products of this radar are distributed free of charge. Any user can download them through the web platforms of the Alaska Satellite Facility or the ESA. The images could be acquired in four modes (Extra Wide Swath, Strip Mode o modalidad de franja, Wave Mode y Interferometric Wide Swath) and with a spatial resolution that depends on the level of processing applied to the product.

The images used in this project were acquired with the Interferometric Wide Swath mode, the default acquisition mode over land and a Ground Range Detected (GND) processing level with High Resolution; this processing level has a terrestrial projection using an Earth ellipsoid model. Phase information is not preserved.

The study area is covered by two scenes, the upper scene with ascending orbit and the lower scene with descending. In order to analyse the dynamics of changes during one year, 12 images were downloaded, one for each month analysed, within each of the scenes covering the study area.

All images have a spatial resolution of 10 metres and are composed of four bands, two Amplitude bands (VV and VH) and two bands with intensity information (VH and VV).

Twenty-four images were analysed with acquisition dates between November 2020 and November 2021, as shown in Table 2.

Orbit	Acquisition time			
Ascendent	11 Nov 2020	05 Dic 2020	10 Jan 2021	03 Feb 2021
	04 Apr 2021	10 May 2021	03 Jun 2021	09 Jul 2021
	02 Aug 2021	07 Sep 2021	13 Oct 2021	30 Nov 2021
Descendent	20 Dec 2020	17 Jan 2021	10 Feb 2021	18 Mar 2021
	23 Apr 2021	05 May 2021	10 Jun 2020	16 Jul 2021
	09 Aug 2021	02 Sep 2021	08 Oct 2021	13 Nov 2021

Table 2. Acquisition time for Sentinel 1 images

5.2.2 TerraSAR-X and TanDEM-X

" TerraSAR-X and TanDEM-X are “twins” German satellites launched in June 2007 as a product of a public-private partnership between the German Aerospace Centre (DLR) and EADS Astrium GmbH" ((Buckreuss et al. 2009, p. 1).

These radars use SAR technology to capture images of the entire planet with a revisit period of 11 days.

Using the X-band and capturing information in two polarisations generates images with high spatial and radiometric resolution.

These characteristics have made it one of the best tools for analysis and monitoring the Earth in areas of high cloud cover. Images can be acquired in different basic modes that depend mainly on polarisation and geometric projection.

The DLR provided the images analysed in this project under a purely academic use agreement. For the study area, an archive image captured by the TanDEM-X satellite was found to be available Table 3.

Specification	TanDEM-X
Acquisition time	21 julio 2021
Acquisition orbit	Ascending
Imaging mode	StripMap
Polarisation	HH (Single)
Data product	Single Look Slant Range Complex (SSC)/L1B
Resolution mode	3.2 meters

Table 3. TanDEM-X images specifications

5.2.3 Reference data

The baseline data used to evaluate the results were provided by the SIMCI project of UNODC in Colombia. These data were supplied as polygons in vector format and correspond to the areas affected by alluvial gold mining in the study area in 2021.

5.2.4 Software description

The development of this project was mainly used the open-source software SNAP, a tool developed by ESA to support the Sentinel missions. It consists of several modules for the processing and visualisation of radar satellite images.

Through the Sentinel-1 toolbox, image pre-processing (thermal noise reduction, radiometric and geometric calibrations, speckle reduction, among others) was implemented. The processing was also performed with this toolbox by implementing time series, texture analysis and supervised image classification.

ERDAS Imagine 2020 was used to edit the classification by removing loose pixels and applying filters to improve the results. The final classification mosaic was performed using this software since each scene was classified independently.

Additionally, with ArcGIS Pro version 2.7, was carried on the analysis of the distances of areas classified as affected by the water bodies to zones with affectation in the year 2021 (according to the reference data), and the height using the elevation mask generated with the metadata of the images.

5.3 Image pre-processing

Sentinel-1 images with coverage over the study area were identified and downloaded at this stage.

Additionally, algorithms for radiometric and geometric correction of the images were defined and executed, and the subset was performed to reduce the effective area to be analysed.

This step is essential to generate images in which the value of each pixel is directly related to the backscatter of the scene. This procedure guarantees the comparability of the images acquired at different times and makes possible the quantitative analysis of the images. For the pre-processing, an automated workflow was created using the Graph Builder tool of the SNAP software, which defined the sequence of image preparation and correction operations, as shown in Figure 8.

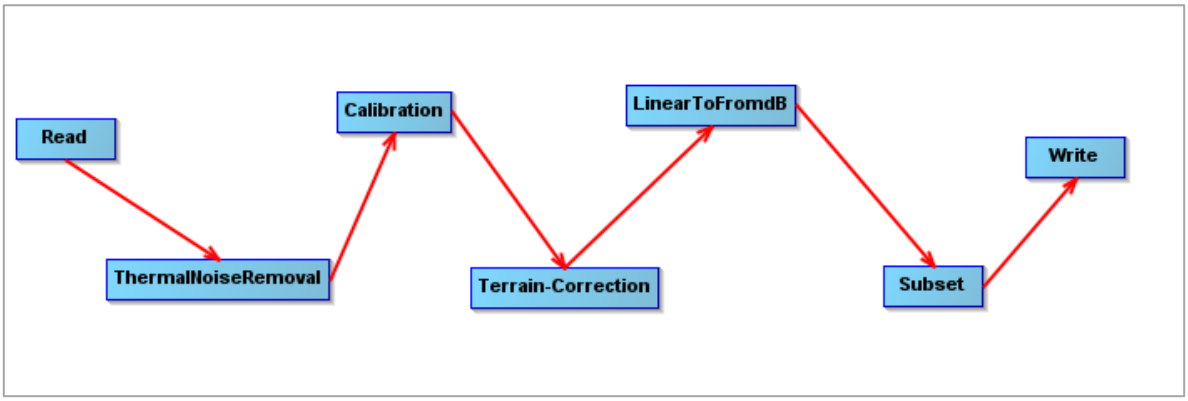

Figure 8. Pre-processing Sentinel 1 workflow

5.3.1 Thermal Noise Removal

Thermal noise is the additive background energy that causes a noise floor and mainly affects the cross-polarised bands since the depolarised power of these bands is weaker than the initial polarised power (Park et al. 2016). The correction of this noise is required to analyse the cross-polarised bands (VH and HV).

For the correction was applied the SNAP algorithm which uses the information of the calibrated noise vectors stored in the metadata of the image. Figure 9 shows a detail of the image before and after applying the noise reduction in the band with cross-polarization. The main difference can be seen on the water surface since by reducing the thermal noise, the mixing of pixels or mottling effect on this surface is reduced, and the water land cover has a more homogeneous appearance.

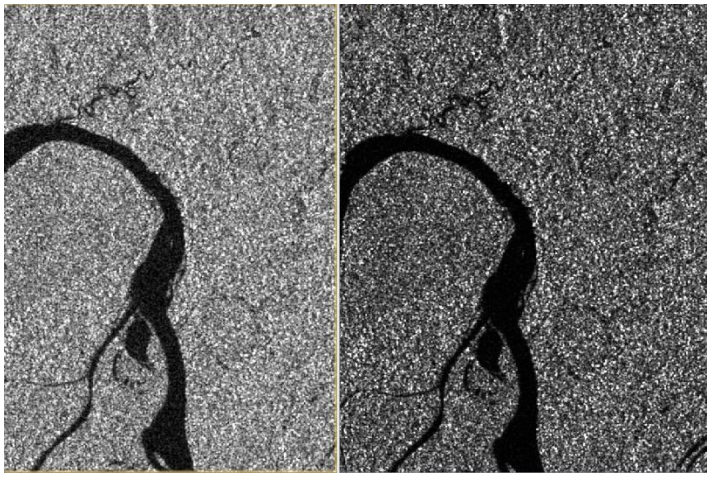

Figure 9. Left: original image VH band. Right: image without thermal noise VH band

5.3.2 Radiometric calibration

The Sentinel 1 images used have processing level L1, this level does not include radiometric calibrations, and therefore it is necessary to apply a correction in order to the pixel values represents the radar backscatter of the reflecting surface. This procedure aims to correct distortions due to signal loss in propagation, the non-uniform radiation pattern of the antenna, and differences in gain and saturation changes.

This allows the generation of images in which the pixel values are directly related to the backscatter of the radar in that scene. This process is essential so that images acquired with different sensors or with the same sensor at different times are comparable, and the quantitative results obtained for the different time points are also comparable.

The radiometric calibration of the images was performed with the correction method of the SNAP software, and the Sigma correction was applied to the two intensity bands. As a result of this correction was generated an image with the backscatter returned from a unit area on the ground, this calibration is useful to interpret the scattering and reflection of the surface and its properties.

Once the calibration was applied, the images with different capture times can be compared. This ensures that the images can be used as input to the same classification and the proper construction of time series.

5.3.3 Speckle reduction

Radar images have a characteristic noise known as salt and pepper, this speckle causes a constructive and destructive variation in the backscatter intensity that affects the quality of the image and, therefore, of the products generated from it.

Different types of filters have been developed to reduce this effect and ensure better homogeneity in the backscatter intensity of the image. Speckle reduction processes apply resampling methods that modify the original spatial resolution image. Considering this, the selection criterion for the most optimal method is given by the highest noise reduction with the lowest possible loss of spatial resolution.

Three methods were tested for speckle reduction:

a. **Single Product Speckle filter:** filters defined in a kernel window are applied with this method. The type of filter and the size of the kernel determine the amount of reduced noise and the level of decrease in the spatial resolution of the image.

   This work were explored 3 of the filters available in SNAP: Lee, Lee Sigma and Median filters. All filters were applied with 3X3, 5x5 and 7x7 kernels and the Lee filters with a Look.

   The median filter (3X3 kernel) obtained the best visual results since it generates an image with a lower noise level than the original. Although the spatial

resolution is reduced, the details of the coverages of interest, such as the limits of the water bodies or streams of the main river and surrounding areas without vegetation, are preserved.

On the other hand, the Lee and Lee Sigma filters generated considerably more blurred images than those obtained with the Median filter. The filters applied with 5x5 and 7x7 kernel generate a more significant speckle reduction, however, they also reduce the resolution, and the result is blurred images with a high level of loss in the details of certain coverages, especially of small water bodies (beneficiation ponds) that are important for the analysis in this work. Figure 10 shows the results obtained with three different filters.

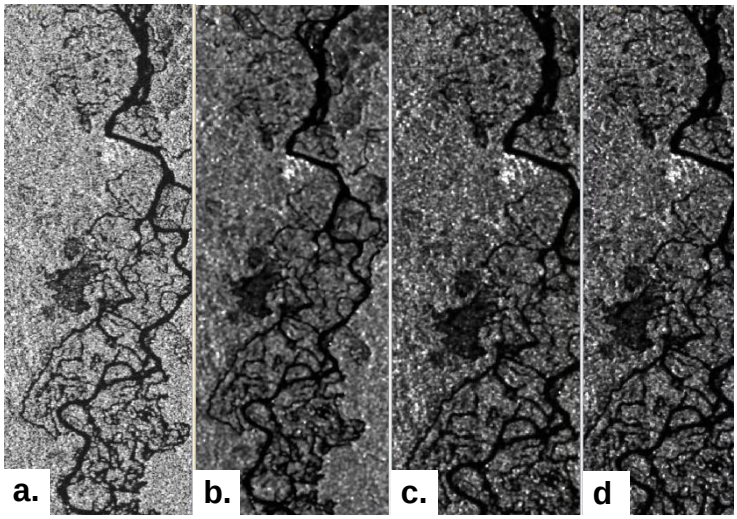

Figure 10. a.Original image. b. Lee Sigma 3x3. c. Lee 3x3. d. Median 3x3

b. Multilooking: this method divides the radar beam into several sub-beams narrower; each sub-beam provides an independent look of the illuminated area. To reduce noise, the algorithm aggregates the different looks and averages them. The result is a noise-reduced image, calculated from the average of the original image values.

This filter was applied before the geometric correction of all images. To explore this method the tool was run in SNAP with different values. The first value used was one look and a value of 20 Mean Square Pixel (MSP). With these values , an image with a spatial resolution of 20 m and considerable noise reduction concerning the original image was obtained.

Additionally, the process was executed with a value of 30 MSP and one look. With these parameters, an image with a spatial resolution of 30 m was obtained, showing a significant noise reduction. However, the decrease in spatial resolution reduces the visibility of elements such as streams or not flowing bodies of water.

Figure 11 shows a detail of the original image and the images resulting from multi looking at 20 m and 30 m, respectively.

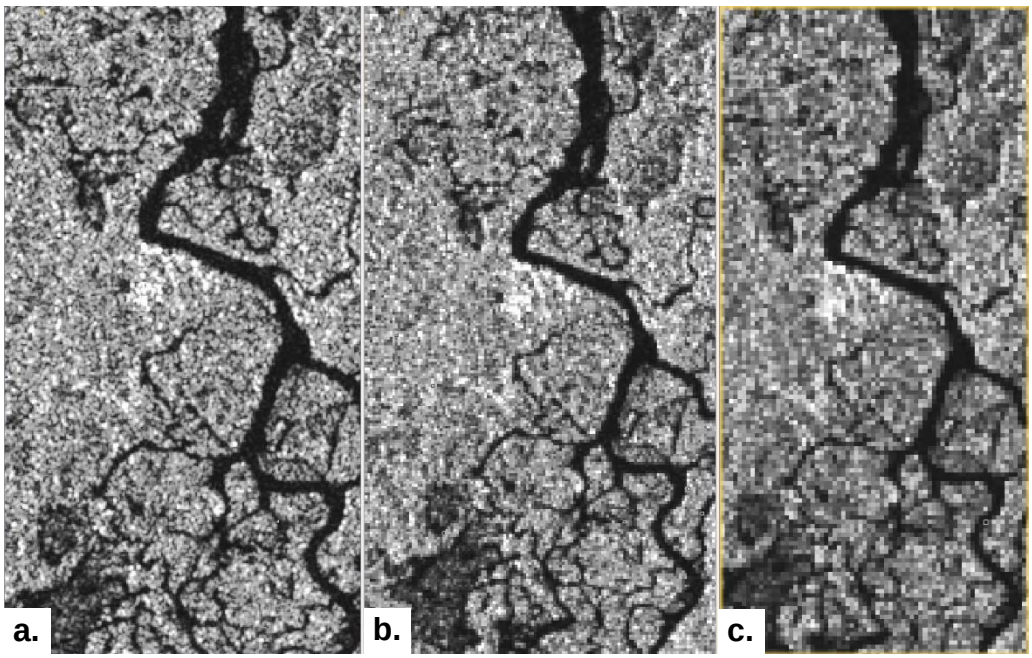

Figure 11. a.Original image. b.Multilooking 20 m. c.Multilooking 30 m

c. **Multi-temporal Speckle filter:** this filter was applied using several images with different acquisition times to eliminate the noise from applying a statistical operation between the values taken by a pixel in the different images.

   To explore this method, 12 images corresponding to the months between November 2020 and November 2021 were used.

   As a result, images with high noise reduction were obtained. However, the spatial resolution was also highly reduced. Additionally, this method uses the average pixel values for the images of all the months included. As a result, the

variation in changes over time is lost, which is an essential factor to analyse to define the growth dynamics of alluvial gold mining extraction.

Figure 12 shows a comparative detail of the original image and those obtained after applying a simple speckle filter and a multitemporal filter. Naturally, the application of this filter also implies the use of a kernel of a minimum size of 3x3. The resulting image has a reduction in the resolution concerning the original image.

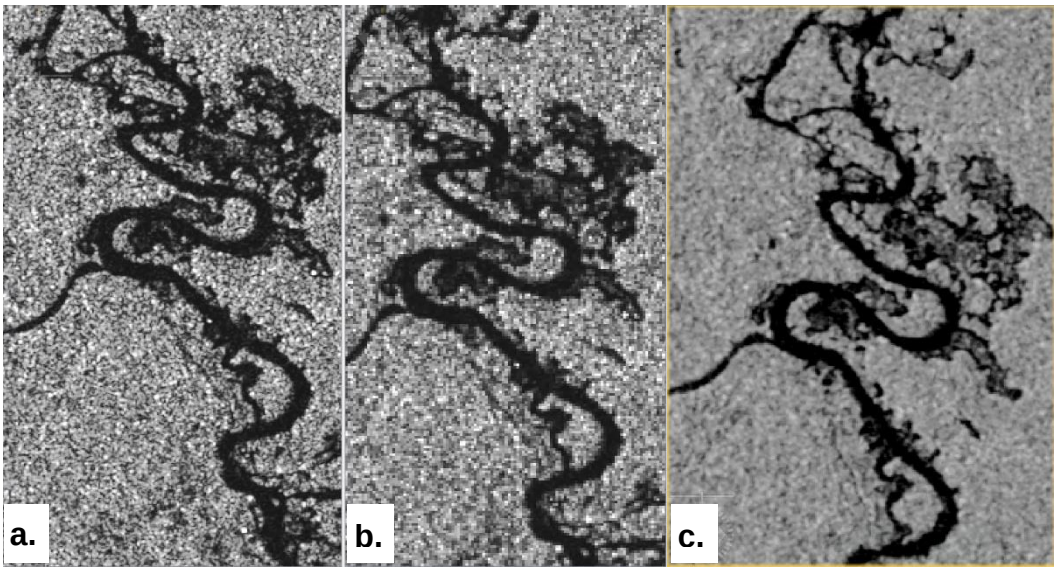

Figure 12. a.Original image. b.Simple filter. c.Multitemporal filter

Exploring the different speckle reduction methods concluded that multi looking has the most suitable results since it is effective in suppressing noise but preserves the edges, details and textures of the main water bodies, the beneficiation ponds and non-vegetated areas. In addition, this method maintains the average levels in the homogeneous regions and allows the visualisation of areas with changes over the time interval analysed.

5.3.4 Terrain correction

Geometric correction is one of the most critical stages of pre-processing since it allows a conversion of the values of the slant range geometry into a map coordinate system. The method used was Range Doppler, which corrects the typical distortions of radar images associated with foreshortening, layover and shadows. The SNAP software uses the topographic information from the Digital Elevation Model and the image file where the satellite orbit and velocity values are defined.

The Digital Elevation Model Shuttle Radar Topography Mission (SRTM) with a resolution of 1 arcsecond (30 metres) was used for image correction. Additionally, Bilinear Interpolation was used for DEM and image resampling and WGS84 as a map projection.

The first of the observable effects after the correction was that the image is oriented in the real direction of the terrain, this makes that the geographic elements are in the correct position, and therefore the image has a completely different orientation than the initial image as can be seen in Figure 13:

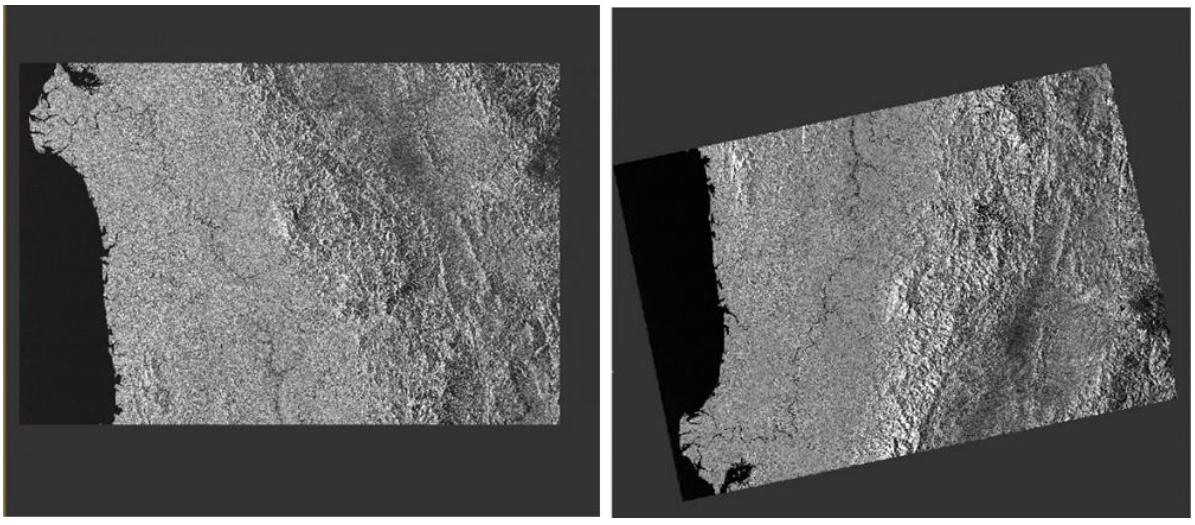

Figure 13. Left.original image. Right.Geometric correction

Three methods of image resampling, bilinear interpolation, cubic convolution and nearest neighbour, were explored for geometric correction. All three methods generated good results with respect to layover correction and foreshortening; however, the bilinear interpolation method provided a better visual reduction of shadow and a less mottled image. Figure 14 shows a detail of the image with the result of the evaluated resampling methods.

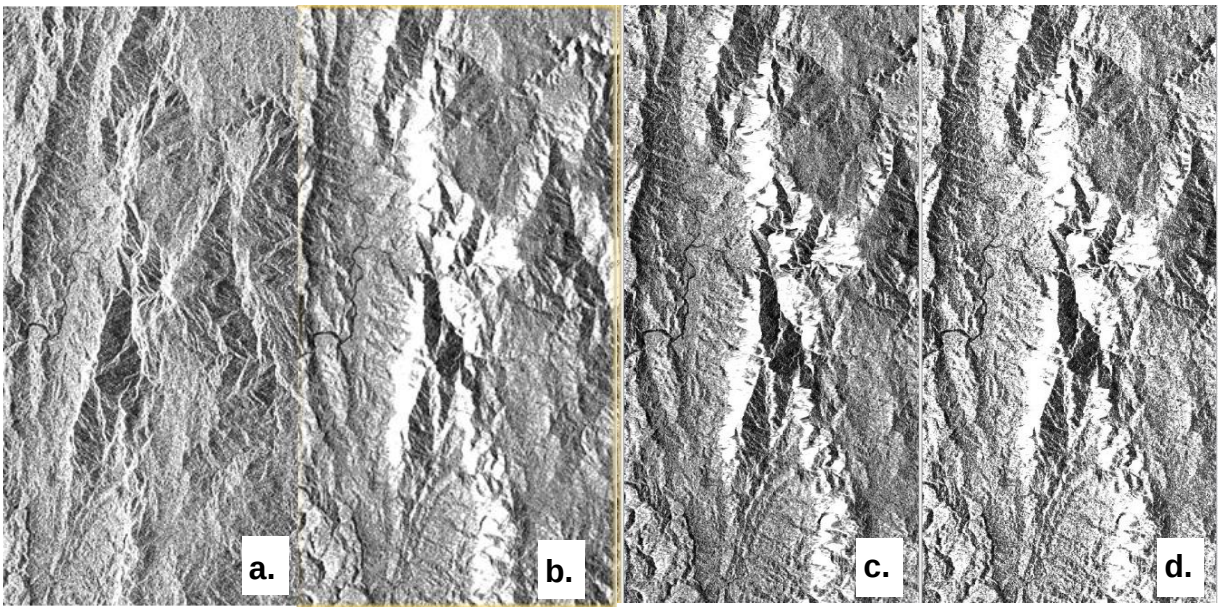

Figure 14. a.Original image. b. Bilinear interpolation. c.Cubic convolution. d.Nearest Neighbour

5.3.5 Linear to db values

The original image has a wide colour range for the distribution of backscattering values so that only very bright objects appear sharp. To improve the visualisation, analysis and comparison, the intensity values were transformed to logarithmic dB values, which guarantees a more homogeneous distribution within the black and white colour tones. This redistribution increases the presence of grey pixels and reduces the number of pixels with extreme values.

Figure 15 shows how in the original image the intensity values are mainly accumulated towards the black and dark grey tones, while in the decibel converted image, the values are better distributed across the whole colour palette so that the

extreme values are closer together, reducing the contrast in some areas of the image and highlighting the structure in the originally darker parts.

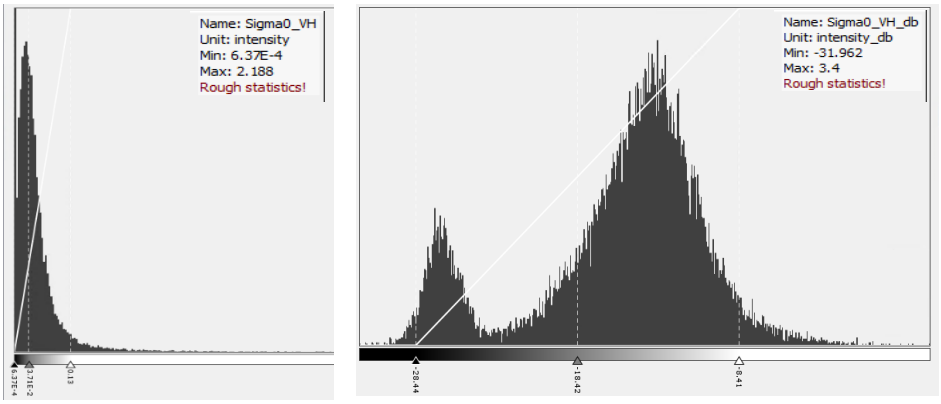

Figure 15. Histogram distribution for Left.Original intensity values.Right. Intensity in decibeles

Additionally, manual manipulation of the contrast can be done by modifying the minimum and maximum values to have visual enhancements that allow better identification of some elements that are not entirely identifiable in the original image.

5.3.6 Subset images

Once the pre-processing was done, all the images were subset taking into account the limits of the study area. This reduces the size of the information analysed and, therefore the volume of data and the processing times used in the analysis.

5.3.7 RGB image visualisation

Combining values with each polarisation in different RGB improves the visual identification of elements that are not differentiable by individual band analysis. After experimenting with different combinations, it was identified that the optimal combination to visualise different land covers is the VV intensity in the red channel, VH intensity in the green channel and the subtraction of the VV intensity/VH intensity in the blue channel.

5.4 Image processing

This subsection describes the stages implemented to process the images and produce the final results.

5.4.1 Multitemporal stack

This process allows storing images from different acquisition dates in a single file. All the images contain the backscattering intensity information calibrated in VH and VV polarisations and all the bands are geocoded with the same projection (WGS84). A stack is created with all the images that will be part of the time series.

For this, it is essential that all images have been acquired with the same orbit (ascending or descending) and that they have been radiometrically and geometrically corrected. Two multitemporal stacks were created for the analysis, one of them with the images acquired with ascending orbit and the other with the images obtained with descending orbit.

As a result of the multitemporal stack, a single file is obtained containing the two bands (VH and VV) of the images for all the analysed acquisition dates.

5.4.2 Time series analysis

Time series allows the visualisation of changes by assigning different dates or points in time to each of the RGB bands of an image. With time series, each colour channel represents whether the area has high backscatter at the acquisition date assigned to that channel.

In the compositions performed, land covers that do not present changes during any of the analysed months maintain the same grey tone in all images; this behaviour occurs, for example, in areas of forest that were not intervened or in areas that were affected by alluvial gold mining before the initial analysis date (November 2020).

Areas with water bodies are consistently dark because they have low backscatter at all times analysed. The red, yellow, blue and green tones represent areas with changes in the acquisition date assigned to the channel with the respective colour.

Figure 16 shows how the backscatter intensity changes in the areas that changed (loss of forest, increase or decrease in the presence of water) with an RGB combination for three different periods.

This temporal signature allows locating the areas with changes in the land cover during the analysed period; this was the first step performed to identify possible affected areas and classify them using two thematic categories: changing or stable areas.

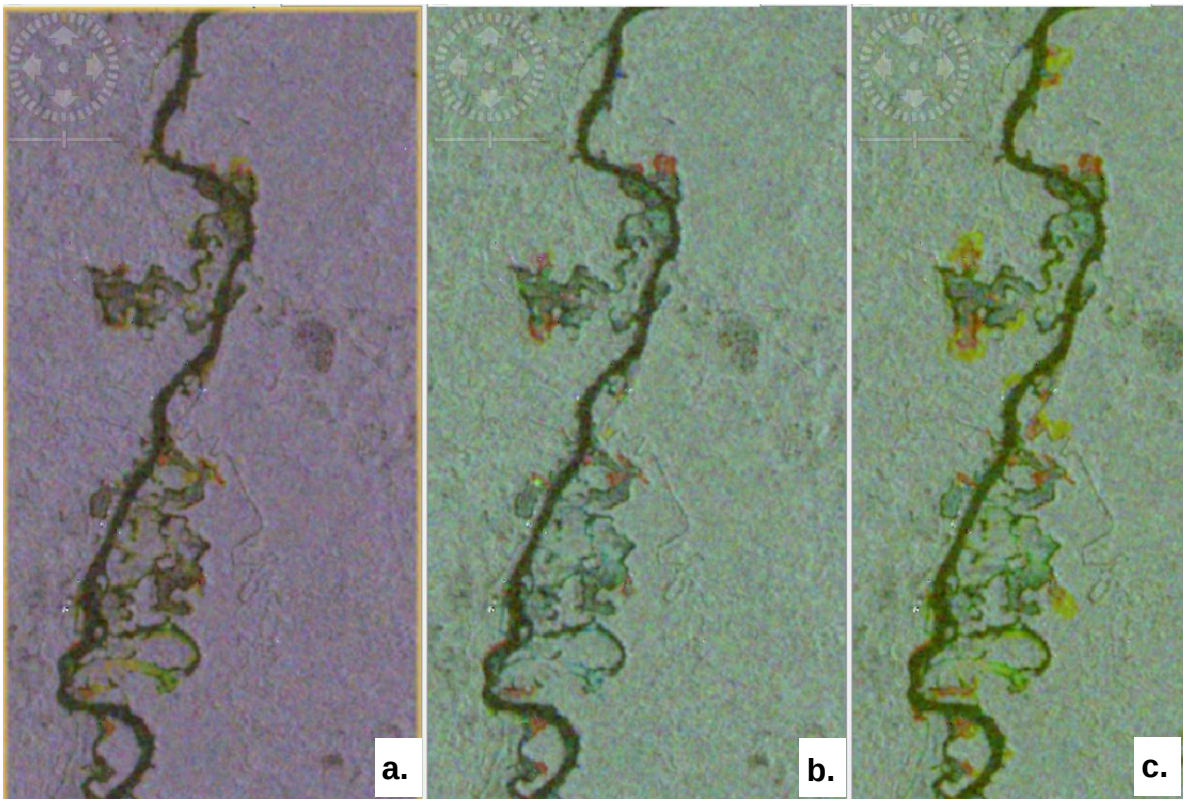

Figure 16. RGB composition for a.3 months, b.6 months, c.12 months

Additionally, the backscatter values for pixels of different land covers in the image were identified using the time series tool, allowing the selection of training areas to classify the image according to the presence or absence of changes. Samples were collected from different land covers to identify backscattering variation over time and to define whether it corresponds to an area with changes or a stable area.

In graphs a and b of Figure 17, decibel values are shown for vegetation and water bodies covers; although slight variations are observed, the decibel values remain constant throughout the time series.

On the other hand, graphs c and d show the variation in decibel values for two areas with changes. The graphs show how the decibel corresponded to vegetation value at the beginning of the series; however, two or three months later, these values began a continuous reduction throughout the time series. This behaviour indicates a dynamic of vegetation loss in these areas.

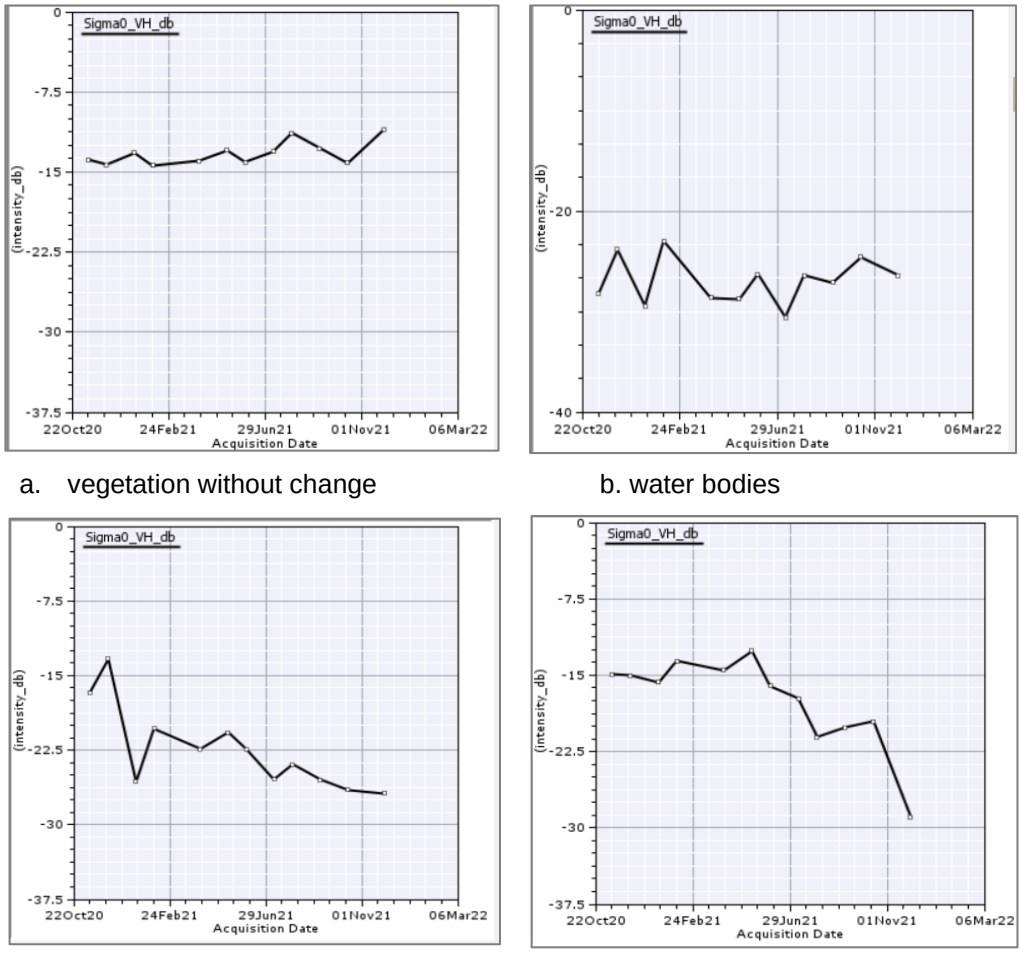

a. vegetation without change

b. water bodies

c. Land cover with changes since Feb 2021

d. Land cover with changes since June 2021

Figure 17. Variation in backscattering for land covers in the study area

5.4.3 Display time-series of entire polygons / working with vectors

Polygons of different land covers to be included as training areas in the classification were defined using the container vector creation tool. The mean was the statistical analysis used to obtain the signatures and identify the training areas for the two classes described in

Table 4.

Class	Description	The pattern in the radar image
Stable covers	Corresponding to areas where there were no changes during the time series analysed. Among these are vegetation characterised by having homogeneous tone and texture in a temporal RGB composition. Also included in this category are the stable water bodies with dark tones, minor texture and linear spatial patterns, for rivers and streams, or circular as in the case of the beneficiation ponds.	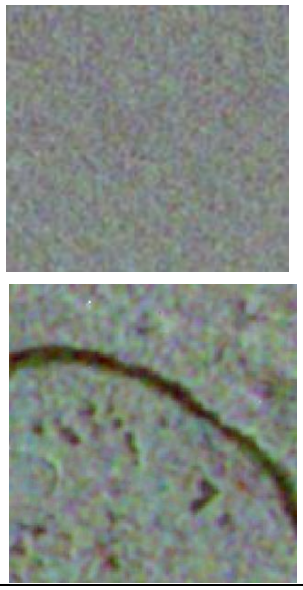
Covers with changes	These are areas that changed at some point in the time series analysed. These areas have tones that range from yellow to red or dark grey tones (depending on the type of cover), with irregular shapes and texture patterns less homogeneous than the areas of stable covers.	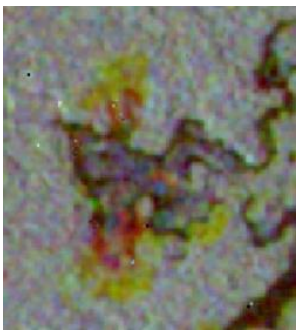

Table 4. Thematic classes change or not change

Figure 18 shows the distribution of values for temporal signatures of each analysed land cover. These polygonal averages are more robust, less susceptible to speckle

and also more representative of the majority of all pixels in a field than individual pixel analysis. As they only represent the averages of all existing pixels, they are not suitable for identifying thresholds. However, these signatures can establish the

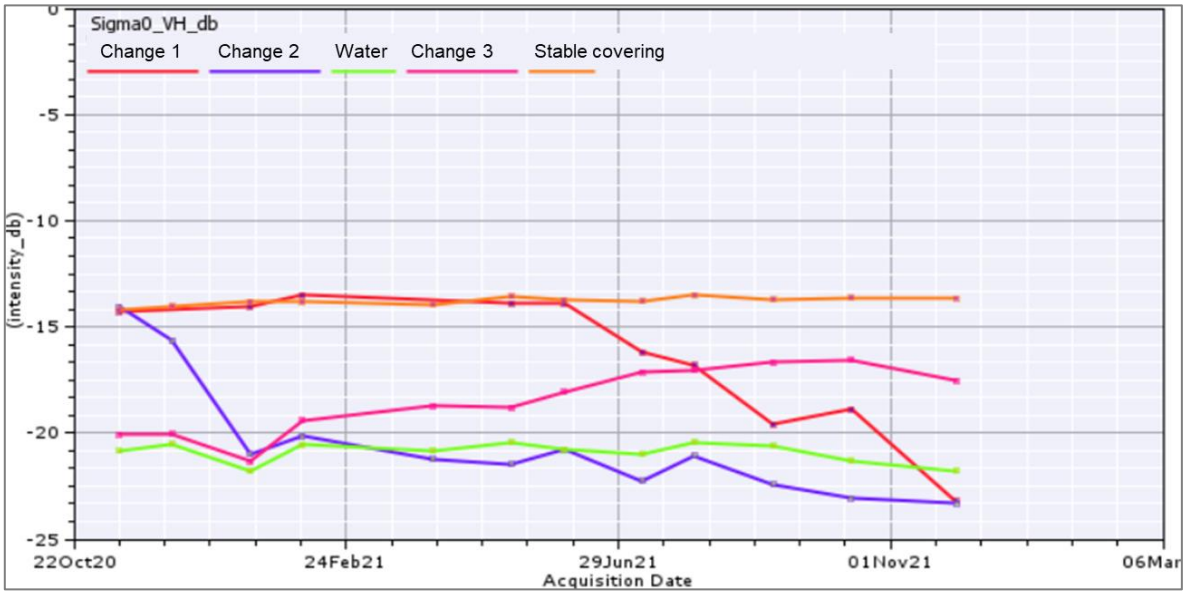

Figure 18. Temporal signature variation for sampled land covers

temporal behaviour of the corresponding cover type.

The plot shows that water bodies and stable land cover had a mean without significant variations throughout the time series. On the other hand, the training areas for land cover changes show variations that reach 15 decibels in some cases. The plot also identifies when the change in the coverages occurs; this is useful for selecting the dates of images to be included in the final supervised classification.

A supervised classification was performed using the Random Forest Classifier algorithm with these training areas, resulting in the distribution of regions with changes and stable regions, Figure 19.

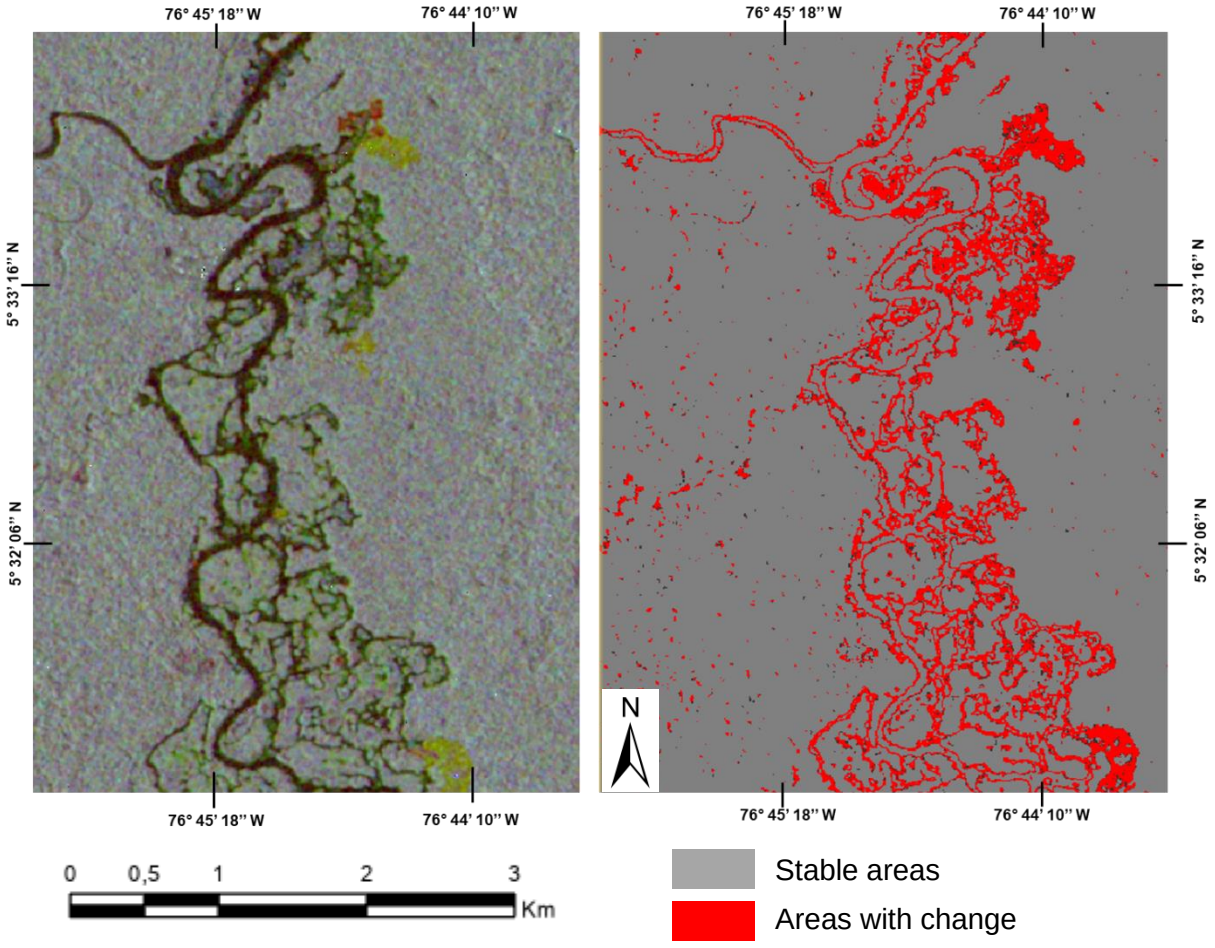

Figure 19. Classification of areas with changes

5.4.4 Supervised classification

To identify the type of coverages that changed, second supervised classifications were performed using the Random Forest Classifier method. The areas with changes previously identified with the time series analysis and the images of the months in which the changes are mainly significant (June to November 2021) were used to define the training areas of the classifier.

The classifications were performed with different polarisation combinations to determine which allow the best identification of possible affected areas.

Classification	No. of bands	Bands included
1	1	VV
2	1	VH
3	1	(VV+VH)/2
4	2	VV, VH
5	3	VV, VH, VV/VH
6	3	VV, VH, (VV+VH)/2
7	3	VV, VH, (VV-VH)
8	5	VV,VH, (VV-VH), (VV/VH), (VV+VH)/2

Table 5. Polarisation band combination used in affected areas classification

Using as mask the classified areas with changes from the time series were taken training seeds for the classes bare soil, water, and other vegetation.

- Bare soil: it corresponds to areas without vegetation. The bare areas associated with alluvial gold mining are located along rivers and streams. These have irregular shapes and finer texture than the areas with vegetation; in some cases, it is possible to observe the cutting line between them and the difference in height with the areas of high vegetation such as forests.

- Water bodies: this cover corresponds to areas with water, like rivers and streams. In areas with alluvial gold mining extraction, these covers also correspond to the presence of small ponds or thin water arms formed due to the deviation of the river.

- Other vegetation covers: this class includes natural forests (predominant cover in the study area), secondary forests and other types of low natural vegetation. Although the analysis of this cover is not the main objective of this work, training areas of this cover were captured to provide differentiation and decision criteria for the classification algorithm.

Visual inspection of the results indicated that classifications performed with a single polarisation contain high noise levels, coming from ground pixels reflected through

vegetation areas with digital values similar to those in bare ground areas. The noise level is higher in classifications run with only VV polarisation.

The noise in the classification decreases as the number of bands and polarisations included increases, so the best results were obtained using the bands VV, VH, (VV-VH), (VV/VH), (VV+VH)/2. Figure 20 shows a detail of the area of interest classified with different combinations of bands.

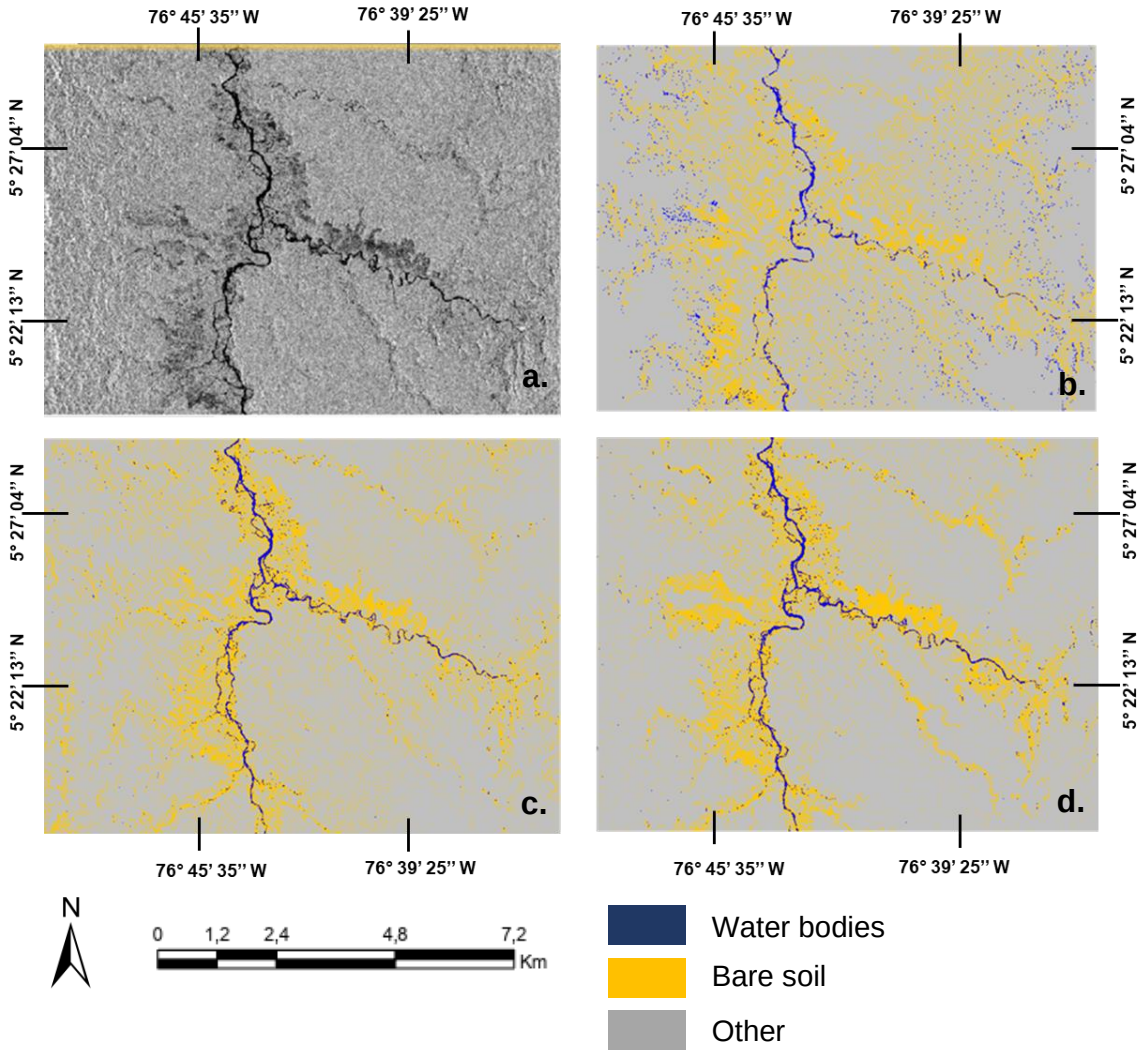

Figure 20. a.Original VH band. b.VH classification. c.VV,VH,(VV+VH)/2 classification. d.VV,VH,VV-VH, VV/VH, (VV+VH)/2

5.4.5 Texture analysis

To identify the impact of the inclusion of textures in the identification of affected areas, the ten texture metrics available in SNAP were generated, including contrast, dissimilarity, homogeneity, energy, Angular Second Moment, Entropy and the Grey Level Co-occurrence Matrix of Mean, Variance and Correlation. From the tests carried out, it was observed that the correlation texture provides better criteria in the differentiation of the boundary for the analysed covers. It presents a better definition of the water bodies and their boundary with the surrounding areas, as shown in Figure 21. Comparison of grey level co-occurrence matrix results

.

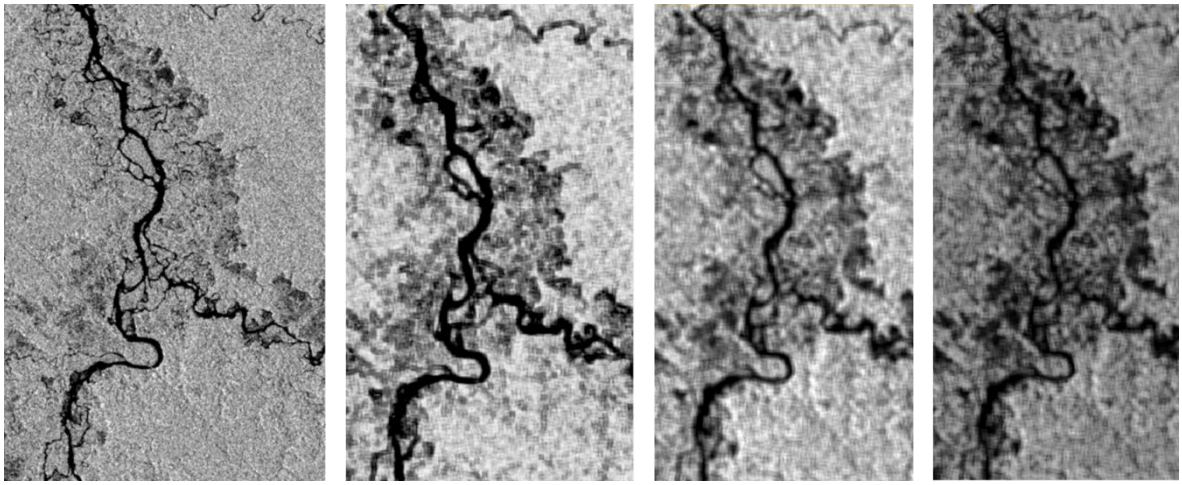

a. Original image *b.Correlation* *c.Mean* *d.Variance*

Figure 21. Comparison of grey level co-occurrence matrix results

Subsequently, different RGB combinations were explored with the correlation of the two polarisations . It was identified that better results were obtained including the combination of RGB (VVCorrelation, VHCorrelation, VVCorrelation-VHCorrelation) as bands in the thematic classification.

For the final identification of bare soil in affected areas, two supervised classifications were performed, including the eight bands listed in table kk for the first and last month of the time series (November 2020 and November 2021). This

classification was performed only within the areas identified with changes from the time series analysis.

Source	Band
Intensity dB values	VV
	VH
	VV-VH
	VV/VH
	(VV+VH)/2
Correlation values	VV
	VH
	VV-VH

Table 6. Band combination used in the final classification

5.4.6 Spatial analysis

As a result, areas without vegetation or bare soils were identified, different activities may have generated these areas. To determine which of these unvegetated areas were associated with alluvial gold mining affectation were performed a spatial analysis using three criteria:

1. Distance to previously affected areas: UNODC in Colombia has defined that the dynamics of the expansion of alluvial gold mining in Chocó is occurring at distances between 80 and 500 metres from the existing affected areas. Based on this analysis, a conservative distance of 80 metres was assumed concerning the limit of affected areas during the year 2021 (United Nations on Drugs and Crime. SIMCI 2016, p. 92), thus defining that the pixels of bare soil located within this distance corresponds to alluvial gold mining.

2. Proximity to water bodies: to assess this criterion, an area of influence of 150 metres to water bodies susceptible to being affected by alluvial gold was defined.

Bare soil pixels within the distance analysed were considered to be the result of alluvial gold mining. In contrast, bare soil pixels outside this distance were deemed to be associated with other deforestation activities.

3. Elevation: to evaluate this criterion, the elevation mask was generated using the metadata of the images and the reference information provided for the year 2021. In this way, it was identified that the areas affected by alluvial gold mining in this region are below 160 metres in elevation.

For the evaluation of the three criteria, a decision tree was defined and is shown in Figure 22.

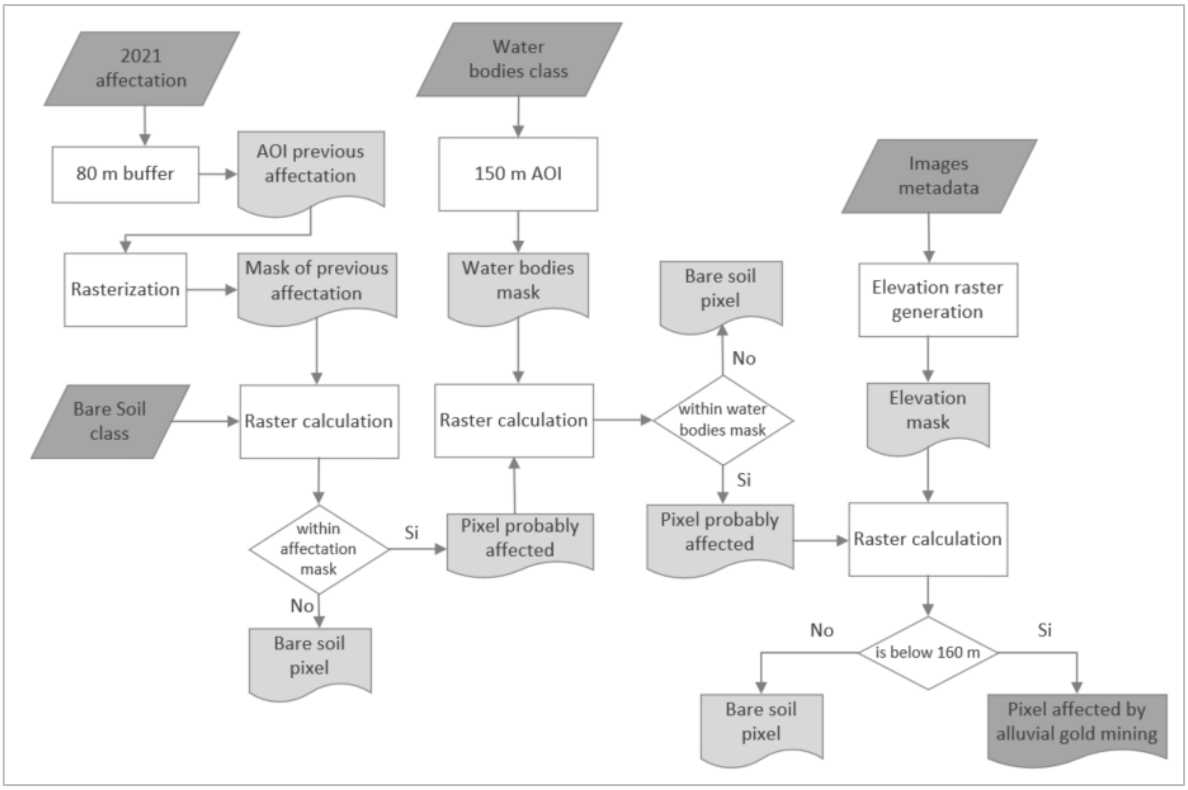

Figure 22.Spatial analysis workflow

5.5 Post procesamiento

This stage was performed with ERDAS Imagine software, by which filtering methods were applied to refine the classification results and remove disconnected pixels.

Additionally, a thematic mosaic was created with the classification of the two Sentinel 1 scenes processed.

5.5.1 Accuracy assessment

For the accuracy assessment, the outputs of the final classification were compared with the 2021 reference data provided.

Although training areas for the classes water, bare soil and other vegetation were included during the classification, the quality assessment was only carried out for the alluvial gold mining affectation. The exclusion of the other classes was done considering that the reference data does not contain reference information for the other classified land covers.

To calculate the accuracy of the prediction of class "alluvial gold mining affectation", the polygons of the reference data were imported into the SNAP and compared with the classification results.

For this process, two masks were created using the Mask Manager tool and the confusion matrix was evaluated as presented in Table 7.

	Affectation	No Affectation	Total	User accuracy
Affectation	665.125	250.981	**916.106**	**73%**
No Affectation	740.096	34.789.895	**35.529.991**	**2%**
Total	**1.405.221**	**35.040.876**	**36.446.097**	
Producer accuracy	**47%**	**99%**		

Table 7. Confusion matrix for affected areas classification

Overall accuracy = 97%

5.6 TerraSAR analysis

5.6.1 Identification of affected areas

The identification of the TerraSAR-X images was done through DLR's EOWEB GeoPortal and the request was made by sending a proposal with the purpose of use and the technical characteristics of the image.

For the pre-processing of the TanDEM-X image (HH polarisation), radiometric calibration, geometric correction and noise reduction with the multi looking method were applied. Subsequently, a subset of the image was performed using an area with alluvial gold mining affectation, previously identified with Sentinel-1 images. Finally, the intensity values were converted to decibels.

Extraction of the ten texture options available in SNAP was performed during processing. By visual inspection of the results, it was identified that the individual texture bands do not provide adequate differentiation of the affected areas; however, using the RGB (Correlation, Variance, Max) combination, areas without vegetation can be observed with fine textures and intense orange tones.

Additionally, the application of different morphological filters (erosion, dilation, open and close) to the texture bands was explored to evaluate the result with respect to the highlight of the boundaries. The figure shows the results obtained with the different filters using the RGB combination (Correlation, Variance, Max). As a result, better visual discrimination was obtained with the dilation filter as shown in the Figure 23.

In this step, the elevation mask was also generated using the image metadata Figure 24. The image of the complete mask can be seen in Appendix 1.

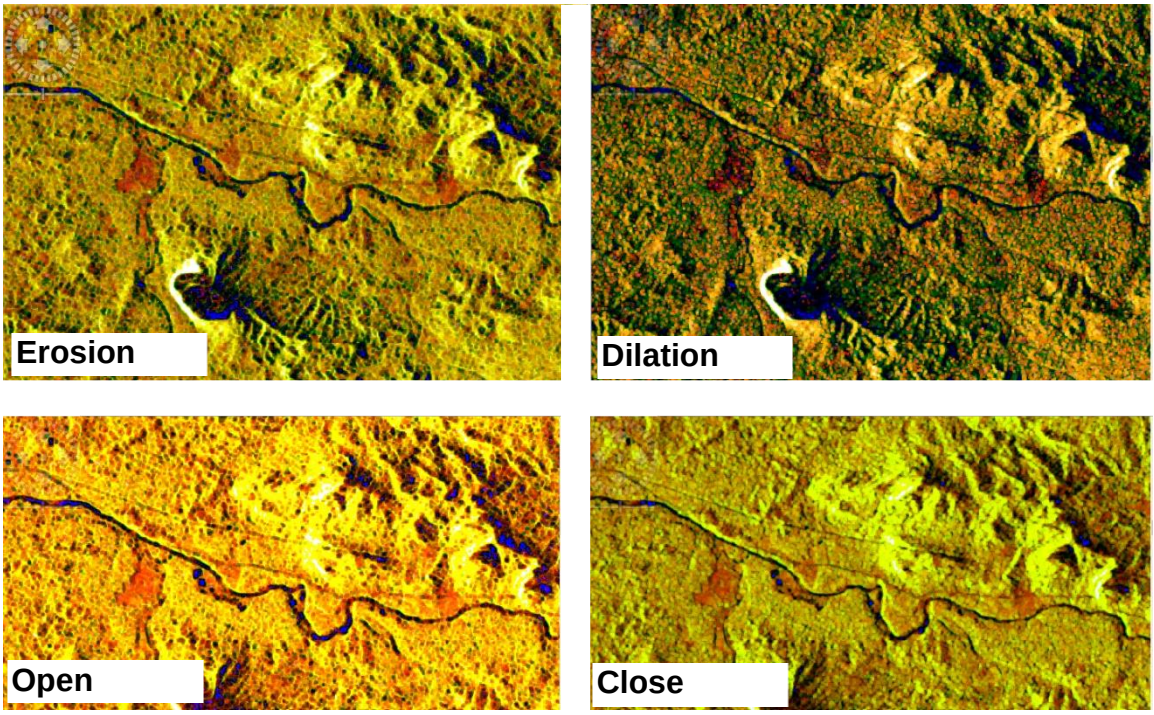

Figure 23. Morphological filters

Finally, a supervised classification was carried out with bare soil, alluvial gold, water and other cover classes, using the bands:

- HH_db
- HH_db_correlation_dilation
- HH_db_variance_dilation
- HH_db_Max_dilation
- Elevation mask

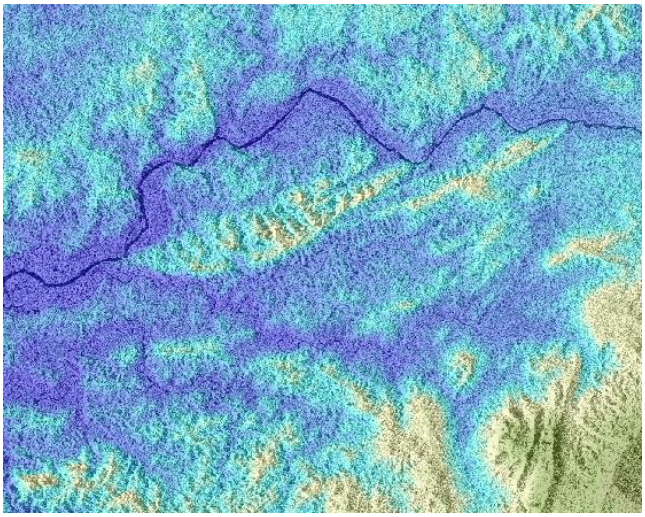

Figure 24.Elevation mask detail

5.6.2 Amazon Analysis

As part of an additional analysis, TerraSAR-X imagery was requested and downloaded from a small area of the Colombian Amazon, where UNODC has reported the presence of over-water gold mining, generated using barges with machinery that suppresses the riverbed to extract the gold.

This type of mining does not generate deforestation or bare soil around the rivers, as in the Chocó region; however, it generates a strong impact due to the dumping of mercury into the water and the alteration in the sedimentation levels of the rivers.

The area analysed is located in the department of Amazonas, on the Putumayo river in southern Colombia. TerraSAR-X, single polarisation (HH) images were available for this area. The most recent available dates are 27 April 2014. Figure 25.

Figure 25. Study area of plus analysis

The images were visually analysed to determine whether it is technically possible to identify the barges and slabs on the Putumayo River. To this end, the images were pre-processed following the workflow described for the Sentinel-1 and TanDEM-X images.

Additionally, texture files were generated to define which metrics would allow better visual identification of these elements. The best enhancement of these elements was obtained with the contrast and dissimilarity metrics as shown in Figure 26. These can be used for visual identification or as input for a more elaborate analysis on the subject combining other types of techniques.

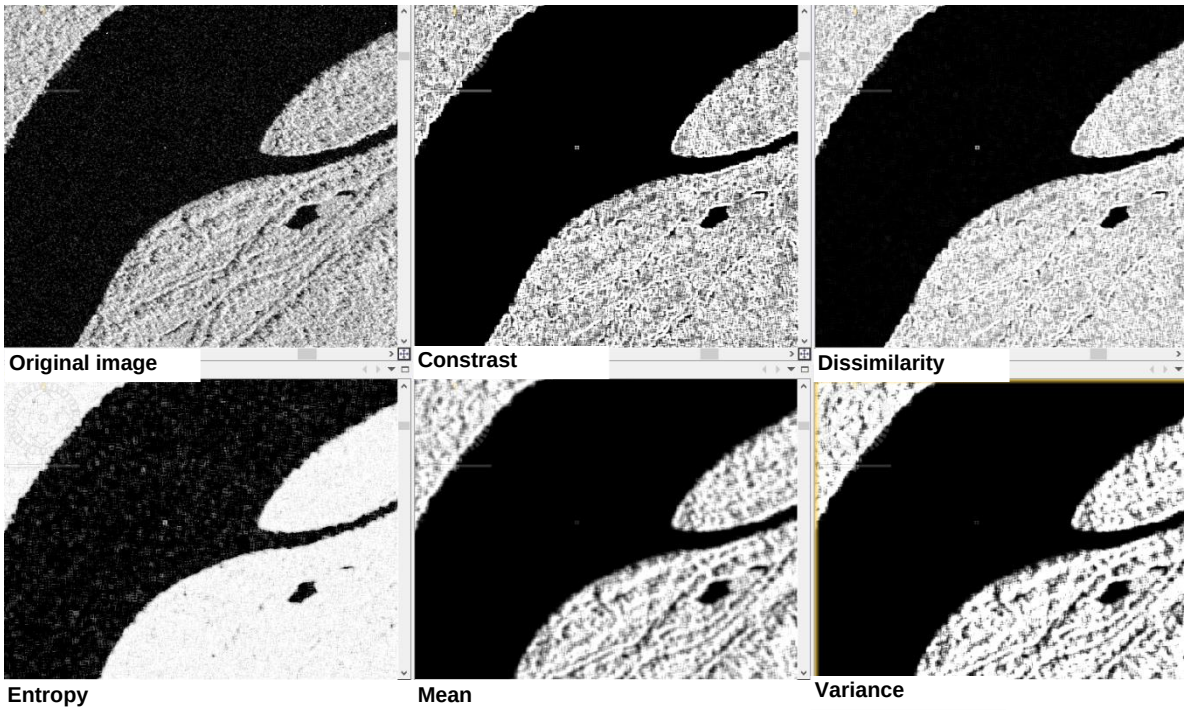

Figure 26. Textures of TerraSAR-X in Putumayo river

6 Results

Using the classification performed was calculated that the alluvial gold mining affectation in the study area in November 2020 was 380 Km^2. In November 2021, it increased to 392 Km^2, representing an increment of 3% per year.

The user accuracy shows that 73% of the affected areas were classified correctly. However, the producer's accuracy (50%) indicates a significant overestimation of these areas.

The overestimation could be mainly associated with:

- The inclusion of areas without vegetation such as sandbanks and river beaches (exposed during the months of less rainfall) which have the same intensity values as the areas affected by mining.

- Differences concerning the reference data (ground truth) may be missing affected areas that were not identified due to cloud limitations of the optical images used for their location.

Using the reference data and the elevation mask was identified that alluvial gold mining in this region occurs below 160 metres.

Figure 28 shows the classification of affected areas and water bodies within the study area analysed.

In the area classified with the TanDEM-X image, an area of 28 Km^2 was identified as possibly affected by alluvial gold mining. The confusion matrix calculated for this classification and shown in Table 8 indicates that 86% of these areas were classified correctly regarding the reference data.

These results indicate better accuracy than with the Sentinel-1 image; this is probably due to the smaller area analysed with the TanDEM-X image. Additionally, this image covers streams of lower water flow, around which the initial expansion of activities that generate vegetation loss occurs. However, this image does not cover areas of the main tributary river around which bare soils are possibly associated with other economic activities.

	Affectation	No Affectation	Total	User accuracy
Affectation	421096	70.756	**491.852**	**86%**
No Affectation	17.015	51.213.998	**51.231.013**	**0%**
Total	**438.111**	**51.284.754**	**51.722.865**	
Producer accuracy	**96%**	**99%**		

Table 8. Confussion matrix for TanDEM image classification

Overall accuracy = 98%

The resolution of the TanDEM-X images allows an adequate identification of water bodies, such as beneficiation ponds, associated with the mining. In the area analysed, 20.000 polygons of small water bodies were identified that probably correspond to beneficiation ponds product of the alluvial gold mining. These water bodies have an average size of 60 m^2 and are located at an average distance of 400 metres from the river around which gold mining is carried out. The final classification is shown in Figure 27.

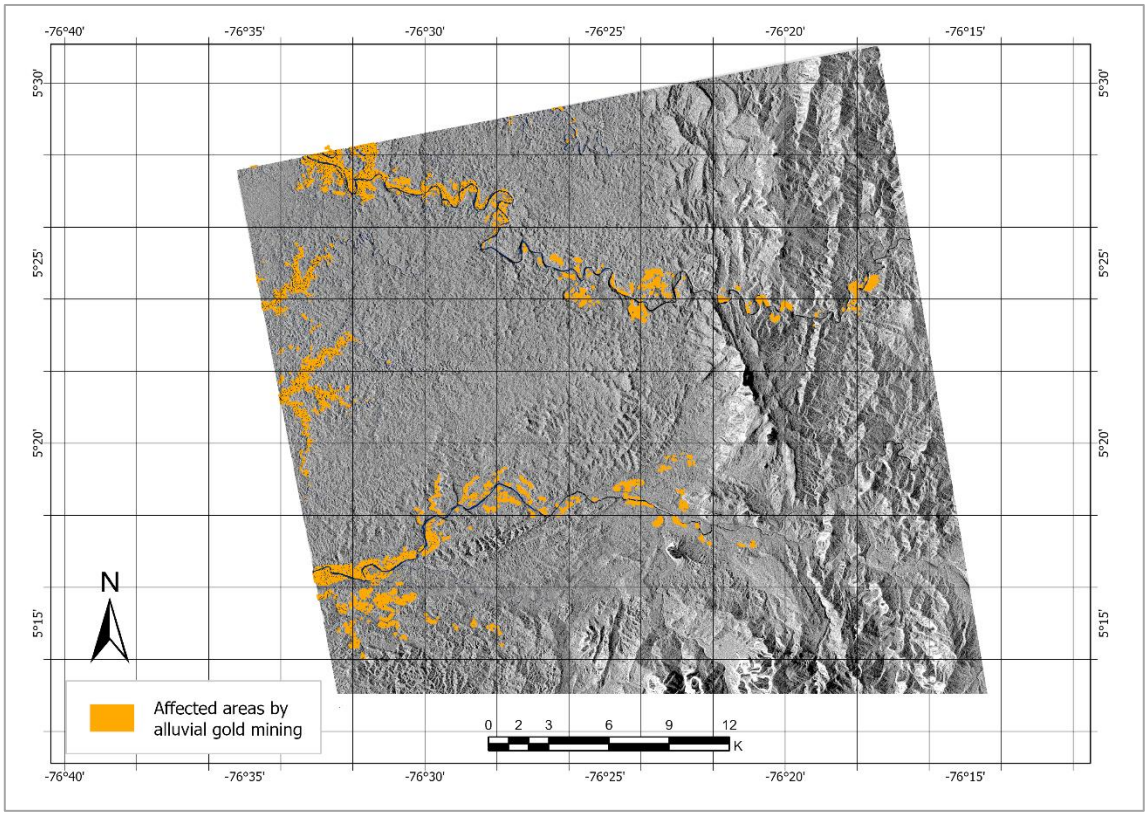

Figure 27. Alluvial gold mining affectation. Image TanDEM-X

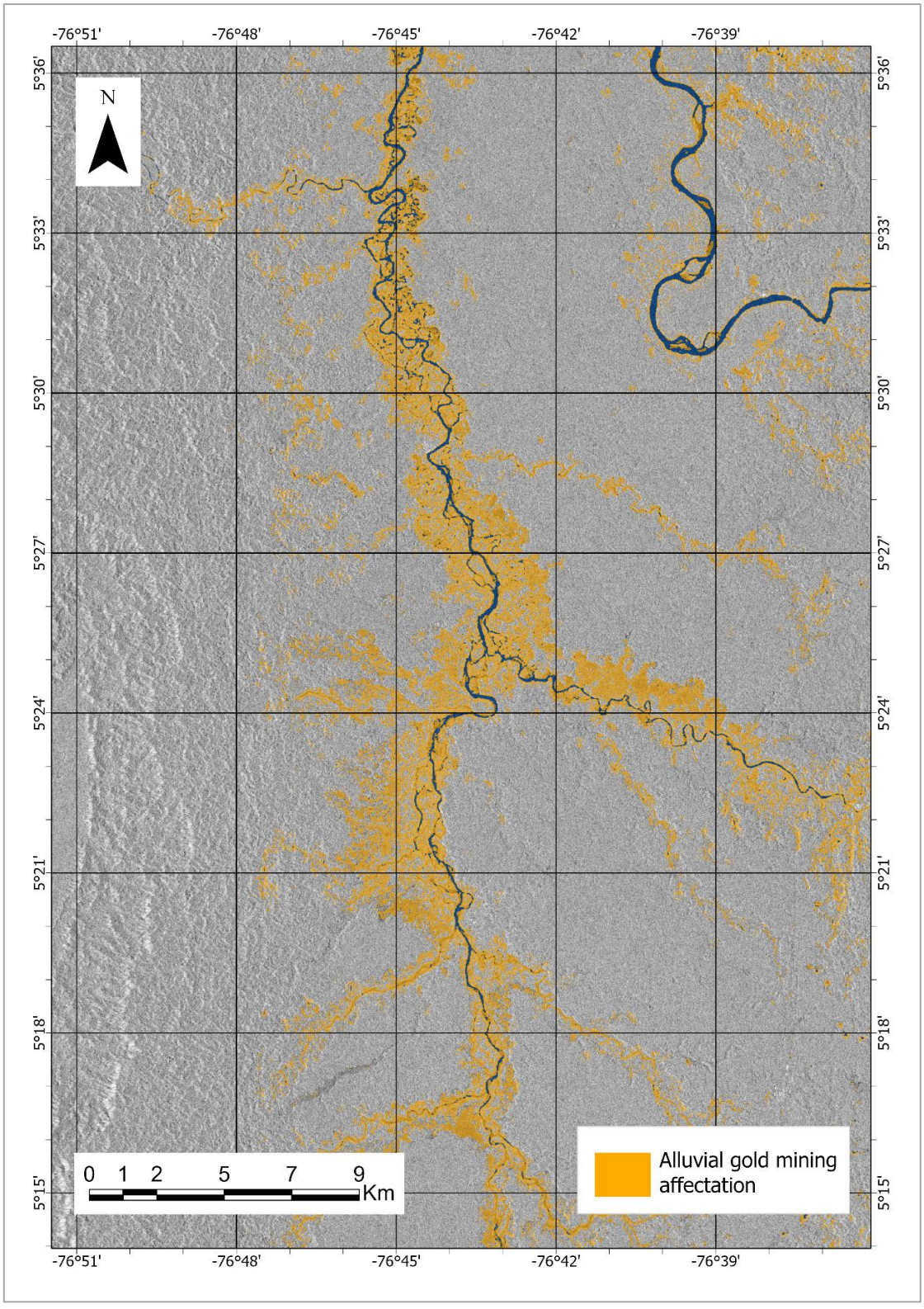

Figure 28. Zoom in on area classified as affected by alluvial gold mining using Sentinel-1 imagery

7 Conclusions

Dual Polarised IW Sentinel-1 images are suitable for rapidly identifying areas affected by alluvial gold mining in regions with high cloud cover. Although good results are obtained, it is necessary to include other criteria of spatial context or specific extraction dynamics to differentiate these areas from bare soils affected by other activities.

A time-series analysis can be successfully used to detect the expansion of affected areas by alluvial gold mining. However, it is essential to note that these are sensitive to changes in flood zones caused by higher or lower rainfall seasons because fluctuations in river flows and river valley flood levels are identified as areas of change in the time series.

Regarding polarisations, the cross-polarisation (VH) channel generates better results than the single polarisation (VV or HH). However, mathematical operations between these allow better differentiation of the affected areas concerning other low vegetation covers.

Sentinel 1 images are helpful for the general identification of water bodies associated with the dynamics of alluvial gold mining (beneficiation ponds and river deviations). However, TamDEM-X images provide better results because the higher spatial resolution facilitates the identification and characterisation of smaller water bodies.

The integration of the elevation mask, generated from the image metadata, as a band in the classification reduces the confusion of water bodies with the shadows caused by the relief. It provides information to the classification algorithm to discriminate between alluvial gold mining and bare soil associated with other activities, generally located towards the steeper slopes.

TanDEM-X single-polarization (HH) images allow rapid discrimination between bare soils around rivers and vegetation areas. However, the use of only this band limits the separability of backscattering values for areas affected by alluvial gold mining. This limitation can be overcome using, as input in the supervised classification, RGB combinations with the bands resulting from applying morphological filters to the texture metrics.

The application of texture metrics on TerraSAR-X imagery is helpful for the visual identification of structures such as slabs and barges on rivers with overwater gold mining. Automatic identification requires processes not explored in this work but are worth pursuing in future projects.

References

Adamek, Katarzyna; Lupa, Michal; Zawadzki, Mateusz (2021): Remote sensing techniques for tracking changes caused by illegal gold mining in Madre de Dios, Peru 25, (accessed 15 September 2021).

Almeida-Filho, R.; Shimabukuro Y. (2010): Detecting areas disturbed by gold mining activities through JERS-1 SAR images, Roraima State, Brazilian Amazon. Available at: https://www.tandfonline.com/doi/pdf/10.1080/014311600750019967?needAccess=true (accesed 13 September 2021).

Arellano Peña, Henry (2004): Clima de la región Pacífica Colombiana. Available at: https://www.researchgate.net/publication/313670709_Clima_de_la_region_Pacifica_Colombiana (accesed 1 September 2021).

Barnabé, Pierre; Elsy, Ibrahim; Jiang, Jingyi; Lema, Luisa; Giuliani, Gregory; Lacroix, Pierre; Pirard, Eric (2021): Cloud and Cloud-Shadow Detection for Applications in Cloud and Cloud-Shadow Detection for Applications in Mapping Small-Scale Mining in Colombia Using Sentinel-2 Imagery. Available at: https://www.researchgate.net/publication/349375756_Cloud_and_Cloud-Shadow_Detection_for_Applications_in_Mapping_Small-Scale_Mining_in_Colombia_Using_Sentinel-2_Imagery (accessed 18 September 2021).

BBC News (2019): El innovador invento del colombiano Santiago Saavedra para detectar la minerEl innovador invento del colombiano Santiago Saavedra para detectar la minería ilegal que fue premiado por Google. Available at: https://www.bbc.com/mundo/noticias-america-latina-48284322 (accessed 12 September 2021).

Breiman, Leo (2001): Random Forests. Available at: https://link.springer.com/content/pdf/10.1023/A:1010933404324.pdf (accessed 27 December 2021).

Buckreuss, Stefan; Werninghaus, R.; Pitz, W. (2009): The German satellite mission TerraSAR-X. Available at: https://www.researchgate.net/publication/224085727_The_German_satellite_mission_TerraSAR-X (accessed 9 December 2021).

Castro, Rafael; Castillo, Andres (2021): Using SAR Data to Monitor the Impacts of Illegal Mining in Istmina, Colombia. Geospace Solutions. Available at: https://www.l3harrisgeospatial.com/Learn/Case-Studies/Case-Studies-Detail/ArtMID/10204/ArticleID/24074/Using-SAR-Data-to-Monitor-the-Impacts-of-Illegal-Mining-in-Istmina-Colombia (accessed 15 September 2021).

Conservacion Amazónica-ACCA (2021): Radar Mining Monitoring-RAMI. Available at: https://rami.servirglobal.net/ (accessed 14 September 2021).

Curlander, John C.; Mcdonough, Robert N. (1991): Synthetic Aperture Radar Systems And Signal Processing.

Flores, Anderson; Herndon, Kelsey; Thapa, Rajesh; Cherrington, Emil; Kucera, Lea; Quyen Nguyen et al. (2019): The SAR handbook. Comprehensive Methodologies for Forest Monitoring and Biomass Estimation. Available at: https://gis1.servirglobal.net/TrainingMaterials/SAR/SARHB_FullRes.pdf (accessed 2 September 2021).

Guzmán D.; Ruíz, J. F.; Cadena M. (2014): Regionalización de Colombia según la estacionalidad de la precipitación media mensual, a través análisis de componentes principales. Subdirección de metereología. IDEAM Available at: http://www.ideam.gov.co/documents/21021/21789/Regionalizaci%25C3%25B3n%2Bde%2Bla%2Blluvia%2Ben%2BColombia.pdf/92287f96-840f-4408-8e76-98b668b83664 (accessed 20 November 2021)

Hall-Beyer, M. (2005): GLCM texture: a tutorial. Alberta, Canada. Available at https://prism.ucalgary.ca/handle/1880/51900 (accessed 20 December 2021).

Haralick, Robert M.; Shanmugam K.; Diestein Its´Hak (1973): Textural Features for Image Classification. Available at: http://haralick.org/journals/TexturalFeatures.pdf (accessed 27 December 2021).

Ho, Tin Kam: Random Decision Forests. Available at: http://ect.bell-labs.com/who/tkh/publications/papers/odt.pdf (accessed 20 December2021).

Ibrahima, Elsy; Lemab, Luisa; Barnabéa, Pierre; Lacroixc, Pierre; Pirarda, Eric (2020): Small-scale surface mining of gold placers: Detection, mapping, and temporal analysis through the use of free satellite imagery. Available at: https://www.researchgate.net/publication/343736003_Small-scale_surface_mining_of_gold_placers_Detection_mapping_and_temporal_anal

ysis_through_the_use_of_free_satellite_imagery (accessed 18 September 2021).

IDEAM. Subdireccion de Ecosistemas e Información Ambiental (2015): Sistema de Informacion Ambiental de Colombia. Bogotá, D.C. Available at: http://181.225.72.78/Portal-SIAC-web/faces/Dashboard/Biodiversidad2/bosques/bosquesNatural.xhtml# (accessed 11november 21).

Instituto de Hidrología, Metereología y Estudios Ambientales (2016): Sentinel 1 para la detección y mapeo de cambios por deforestación. Bogotá: Centro Mesoamericano para el intercambio de conocimientos y experiencias forestales. Available at: https://www.youtube.com/watch?v=8RVFSyD14RQ&t=11s (accessed 9 December 2021).

Isidro, Celso; McIntyre, Neil; Lechner, Alex; Callow, Ian (2017): Applicability of Earth Observation for Identifying Small-Scale Mining Footprints in a Wet Tropical Region. Available at: file:///D:/University/Thesis/Literature/remotesensing-09-00945.pdf (accessed 13 September 2021).

Jaelani, L. M.; Nurgiantoro; Putri, R. A. (2018): Analysis of Land Cover change due to gold mining in Bombana using Sentinel 1A Radar Data. Available at: https://journals.sfu.ca/ijg/index.php/journal/article/view/1130/604 (accessed 14 September 2021).

Joshi, Neha; Mitchard, Edward; Woo, Natalia; Torres, Jorge; Moll-Rocek, Julian; Ehammer, Andrea et al. (2015): Mapping dynamics of deforestation and forest degradation in tropical forests using radar satellite data. Available at: https://iopscience.iop.org/article/10.1088/1748-9326/10/3/034014/pdf, updated on 2/15/2015 (accessed 15 September 2021).

L3 Harris TM. Geospatial: Calculate Confusion Matrices. Available at: https://www.l3harrisgeospatial.com/docs/calculatingconfusionmatrices.html (accessed 22 January 2022).

Microimages, Inc (2012): Introduction to interpreting Digital RADAR Images, (accessed 22 December 2021).

Park, Jeong-Won; Korosov, Anton A.; Babiker, Mohamed; Sandven, Stein; Won, Joong-Sun (2016): Efficient Thermal Noise Removal for Sentinel-1 TOPSAR Cross-Polarization Channel.

The European Space Agency (2021): Sentinel Online. Available at: https://sentinel.esa.int/web/sentinel/missions/sentinel-1 (accessed9 August 2021).

United Nations on Drugs and Crime. SIMCI (2016): Explotación de oro de aluvión. Evidencias a partir de percepción remota 2016. Available at: https://www.biesimci.org/fileadmin/2019/documentos/evoa/evoa-2014.pdf (accessed 9 October 2021).

United Nations on Drugs and Crime. SIMCI (2019): Alluvial Gold Exploitation. Evidences from Remote Sensing 2018. Bogotá. Available at: https://biesimci.org/fileadmin/2019/documentos/evoa/evoa_2018_in.pdf (accessed 9 January 2022).

United Nations on Drugs and Crime. SIMCI (2021): Colombia. Explotación de oro de aluvión. Evidencias a partir de percepción remota 2020. Available at: https://biesimci.org/fileadmin/2020/documentos/evoa/evoa_2020_esp.pdf (accessed 29 Janaury 2022).

United States Agency for International Development (2020): Artisanal and small-scale mining in Madre de Dios, Perú. Perú. Available at: https://land-links.org/wp-content/uploads/2020/11/small.scale_.mining.CS_.10.24.pdf (accessed28 September 2021).

Appendixes

Apendix I. Elevation mask of TanDEM-X image.